

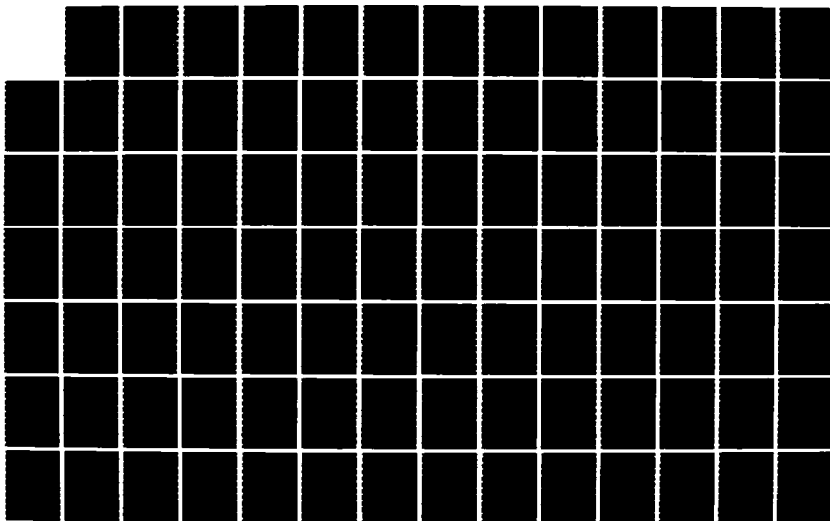
AD-A173 505

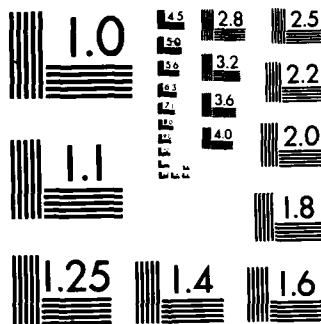
PERSISTENT INFRARED SPECTRAL HOLE-BURNING FOR IMPURITY  
VIBRATIONAL MODES IN SOLIDS(U) IBM ALMADEN RESEARCH  
CENTER SAN JOSE CA A J SIEVERS ET AL 30 SEP 86 TR-7  
N00014-84-C-0708 F/G 14/3

1/1

UNCLASSIFIED

NL





MICROCOPY RESOLUTION TEST CHART  
NATIONAL BUREAU OF STANDARDS-1963-A

AD-A173 505

12

OFFICE OF NAVAL RESEARCH

Contract N00014-84-C-0708

R&T Code 413a001---01

Technical Report No. 7

Persistent Infrared Spectral Hole-Burning for  
Impurity Vibrational Modes in Solids

by

A. J. Sievers (Cornell University) and W. E. Moerner

Prepared for Publication

in

*Persistent Spectral Hole-Burning: Science and Applications*  
(chapter 6), W. E. Moerner, editor, Springer Verlag (in press)

IBM Almaden Research Center  
650 Harry Road  
San Jose, California 95120-6099

September 30, 1986

Reproduction in whole, or in part, is permitted for any purpose of the United States Government.

\* This document has been approved for public release and sale; its distribution is unlimited.

DTIC  
ELECTE  
OCT 24 1986  
S B

DTIC FILE COPY

(12)

SECURITY CLASSIFICATION OF THIS PAGE

ADA173505

## REPORT DOCUMENTATION PAGE

1a. REPORT SECURITY CLASSIFICATION Unclassified		1b. RESTRICTIVE MARKINGS	
2a. SECURITY CLASSIFICATION AUTHORITY		3. DISTRIBUTION / AVAILABILITY OF REPORT This document has been approved for public release and sale; its distribution is unlimited.	
2b. DECLASSIFICATION / DOWNGRADING SCHEDULE		5. MONITORING ORGANIZATION REPORT NUMBER(S)	
4. PERFORMING ORGANIZATION REPORT NUMBER(S) Technical Report No. 7, IBM		7a. NAME OF MONITORING ORGANIZATION Office of Naval Research Chemistry Division, Code 1113	
6a. NAME OF PERFORMING ORGANIZATION IBM Almaden Research Center	6b. OFFICE SYMBOL (If applicable)	7b. ADDRESS (City, State, and ZIP Code) Arlington, VA 22217	
6c. ADDRESS (City, State, and ZIP Code) 650 Harry Road San Jose, CA 95120-6099	8a. NAME OF FUNDING / SPONSORING ORGANIZATION	8b. OFFICE SYMBOL (If applicable)	9. PROCUREMENT INSTRUMENT IDENTIFICATION NUMBER N00014-84-C-0708
8c. ADDRESS (City, State, and ZIP Code)	10. SOURCE OF FUNDING NUMBERS		
	PROGRAM ELEMENT NO.	PROJECT NO.	TASK NO.
			WORK UNIT ACCESSION NO.
11. TITLE (Include Security Classification) Persistent Infrared Spectral Hole-Burning for Impurity Vibrational Modes in Solids			
12. PERSONAL AUTHOR(S) A. J. Sievers (Cornell University) and W. E. Moerner			
13a. TYPE OF REPORT Interim Technical	13b. TIME COVERED FROM TO	14. DATE OF REPORT (Year, Month, Day) September 30, 1986	15. PAGE COUNT 91
16. SUPPLEMENTARY NOTATION Persistent Spectral Hole-Burning: Science and Applications (chapter 6), W. E. Moerner, editor, Springer Verlag (in press)			
17. COSATI CODES		18. SUBJECT TERMS (Continue on reverse if necessary and identify by block number)	
FIELD	GROUP	SUB-GROUP	
		> Persistent spectral hole-burning; vibrational mode; infrared; reorientation.	
19. ABSTRACT (Continue on reverse if necessary and identify by block number)			
<p>One unusual group of excitations in which persistent spectral hole-burning has been observed consists of infrared vibrational transitions of impurity molecules in solids. Examples include 1,2-difluoroethane in rare gas matrices, perhenate ions in alkali halide crystals, and most recently, cyanide and nitrate ions in KBr. The hole formation mechanisms involve molecular reorientation or conformational changes at low temperatures induced by excitation of an internal vibrational mode of the impurity molecule.</p>			
20. DISTRIBUTION / AVAILABILITY OF ABSTRACT <input checked="" type="checkbox"/> UNCLASSIFIED/UNLIMITED <input type="checkbox"/> SAME AS RPT <input type="checkbox"/> DTIC USERS		21. ABSTRACT SECURITY CLASSIFICATION Unclassified	
22a. NAME OF RESPONSIBLE INDIVIDUAL		22b. TELEPHONE (Include Area Code)	22c. OFFICE SYMBOL

86 10 16 170

Chapter 6.

**PERSISTENT INFRARED SPECTRAL HOLE-BURNING  
FOR IMPURITY VIBRATIONAL MODES IN SOLIDS**

A. J. Sievers

Laboratory of Atomic and Solid State Physics, Cornell University, Ithaca, New York 14853

and

W. E. Moerner

IBM Almaden Research Center, 650 Harry Road, San Jose, California 95120

**ABSTRACT:** One unusual group of excitations in which persistent spectral hole-burning has been observed consists of infrared vibrational transitions of impurity molecules in solids. Examples include 1,2-difluoroethane in rare gas matrices, perrhenate ions in alkali halide crystals, and most recently, cyanide and nitrite ions in KBr. The hole formation mechanisms involve molecular reorientation or conformational changes at low temperatures induced by excitation of an internal vibrational mode of the impurity molecule.

Chapter 6.

**PERSISTENT INFRARED SPECTRAL HOLE-BURNING  
FOR IMPURITY VIBRATIONAL MODES IN SOLIDS**

A. J. Sievers

Laboratory of Atomic and Solid State Physics, Cornell University, Ithaca, New York 14853

and


W. E. Moerner

IBM Almaden Research Center, 650 Harry Road, San Jose, California 95120

**ABSTRACT:** One unusual group of excitations in which persistent spectral hole-burning has been observed consists of infrared vibrational transitions of impurity molecules in solids. Examples include 1,2-difluoroethane in rare gas matrices, perhenate ions in alkali halide crystals, and most recently, cyanide and nitrite ions in KBr. The hole formation mechanisms involve molecular reorientation or conformational changes at low temperatures induced by excitation of an internal vibrational mode of the impurity molecule.



Accession	
NTIS	
DTIC	
Uncl	
Just	
By	
Date	
Avail	
Dist	
A-1	



## 6.1 Introduction

### 6.1.1 Matrix-isolated molecules in van der Waals and ionic solids

As was described in the last chapter, the formation of persistent spectral holes by nonphotochemical or photophysical mechanisms has been reported for several inhomogeneously broadened electronic transitions of molecular and ionic impurities in solids in the visible [6.1]- [6.3] . The phrase "persistent IR photophysical hole burning" completely specifies the theme of this chapter. By itself "photophysical" is too general to identify the area of interest here because this phrase is generally used to cover all electronic energy transfer processes in which a chemical bond is not created or destroyed [6.4] whereas, the topic to be considered in this chapter pertains to the small subset of persistent photophysical systems in which no electronic excitation is involved and only vibrational degrees of freedom are photoexcited with infrared radiation. In particular, cases where low temperature IR photochemistry (bond-breaking) occurs and entire inhomogeneous lines disappear are not reviewed here [6.5].

What are the most general requirements for the formation of persistent IR spectral holes (PIRSH's) that last much longer than excited vibrational state lifetimes at low temperatures? In a general sense, the basic requirements for PIRSH formation are three. First, there must be several ground state configurations of the total system, and the IR absorption energies from these ground states must differ by more than the laser linewidth. Second, there must exist an IR pumping pathway that connects these ground state configurations. Finally, the relaxation among the ground states must be slower than the excited state lifetime. If all of these conditions are met, persistent spectral holes may result. A schematic picture of such an IR

induced vibrational process for a molecule at low temperatures is shown in Fig. 6.1. The monochromatic laser source of frequency  $\omega_L$  induces transitions between the  $n=0$  and  $n=1$  vibrational states as represented by the solid vertical lines. In addition to this allowed process there also exists a weakly allowed decay channel (the dotted line) to a different configuration of the molecule-lattice system which is nearly degenerate in energy with the configuration which is being pumped. These two ground states are labeled in the expanded view of the ground state region by the quantum numbers  $c=0$  and  $c=1$ . After many laser-induced cycles some molecules end up in the metastable  $c=1$  configuration, out of equilibrium with the lattice at low temperatures. The large energy barrier separating the two elastic configurations prevents the molecule-lattice system from simply emitting the elastic energy  $\hbar\omega_c$  and returning to the ground state.

To date only a few such persistent IR spectral holes have been reported for low temperature matrix-isolated molecules, but they have been found in solids with two different kinds of bonding: van der Waals [6.6]- [6.8] and ionic [6.9]- [6.13] . These new high resolution measurements are attracting widespread interest not only because they complement earlier results obtained with other spectroscopic techniques on the vibrational spectra of trapped molecular species but also because related persistent effects may occur in the vibrational spectra of solids with other types of bonding.

Spectroscopic research on molecules isolated in the two classes of hosts has been driven forward by different potential applications. Typically, van der Waals matrices of rare-gas atoms have been employed when the interest is centered mainly on the properties of the dopant molecule itself [6.14] [6.15] , such as in the spectroscopic determination of the structure of free radicals [6.16]. This sample preparation technique, which is designed to make the internal vibrational modes of unstable molecules stand out, sometimes obscures the details of the



molecule-lattice interaction. The material to be examined is formed by condensing the molecular and matrix gas on a cryogenically cooled substrate so that the host is necessarily disordered and some ambiguity in the possible arrangements of the nearest neighbors of the dopant molecule results. Although initial measurements did focus on the molecular vibrational modes, it was soon appreciated that a good understanding of the local environment and molecule-lattice interaction would be essential before the static and dynamic properties of the vibrating molecule could be characterized properly [6.14]. Each new advance in spectroscopic technique has continued to resolve more fine structure in the vibrational stretch transitions demonstrating that IR can probe precisely the normal modes of the coupled system [6.17].

The discovery [6.18] of vibrational fluorescence from matrix-isolated CO marked the beginning of a new era in which IR laser probes play a central role in the determination of vibrational energy lifetime and transfer processes for both single and multicomponent molecular species at low temperatures [6.19]- [6.27] . An important result of this work is that molecular rotation plays a key role in determining the excited state vibrational lifetime of diatomic molecules with small moments of inertia [6.19]. Although fluorescence can be measured for most simple molecules, it is much weaker or nonexistent for complex ones, no longer because of rotation but instead due to energy exchange between the anharmonic normal modes. Because complex molecules always contain low frequency modes, nonradiative processes from these low frequency internal modes to external lattice modes of similar frequencies dominate the relaxation, and fluorescence methods cannot readily be used to determine the vibrational lifetime; instead, the more demanding techniques of incoherent saturation and infrared hole burning must be employed [6.28] [6.29] .

Alkali halide host crystals doped with molecules are prepared by diffusion near the crystal melting temperature, pulling a crystal from the doped molten salt (Czochralski-growth) or by

dropping the encapsulated doped melt through a steep temperature gradient (Bridgman-growth). All of these sample preparation techniques limit the possibility of isolating large complex molecules in these single crystal hosts; however, simple molecules can be readily embedded in nine simply related fcc lattices and three bcc ones. Because the electrostatic potential produced at the impurity site by an array of point charges does not contribute to the vibrational frequency of the molecule, one can compare the spectroscopic results obtained for molecules embedded in these matrices with those found for van der Waals solids.

The first infrared measurements on simple molecules in alkali halides were made in 1928[6.30], but the field did not begin to develop until the late 1950's [6.31]- [6.33] . By the early 1970's the complex vibrational spectra obtained for these simple systems had been interpreted in terms of rotational, librational, and tunneling motion of the vibrating molecule as well as local, gap, resonant, and tunneling mode motion of the impurity center of mass in conjunction with the nearby lattice [6.34]- [6.37] . A comparison of the spectroscopic results for diatomic molecules embedded both in ionic and van der Waals hosts has demonstrated that the vibrational dynamics are similar even though the crystal bonding strength is very different [6.37].

The first attempt to determine the energy transfer properties of molecules in alkali halides developed from the desire to make a room temperature saturable absorber for a specific high power  $\text{CO}_2$  laser system using perrhenate ( $\text{ReO}_4^-$ ) ions in alkali halides [6.38]. Low temperature studies on the  $\text{ReO}_4^-$  molecule were initiated when it became evident that long lived vibrational states in matrix-isolated molecules could occur in the  $\text{CO}_2$  laser frequency region. *Gethins* [6.39] had predicted that the local vibrational mode for the  $\text{H}^-$  ion in KBr would have an intrinsic linewidth of 3 MHz due to three- and four-phonon decay processes.

At about the same time *Moos* [6.40] had shown that the multiphonon decay between electronic states in rare earth ions was exponential in the energy gap to the next lowest level. In analogy with these optical results the molecule multiphonon relaxation frequency should decrease exponentially with increasing ratio of vibrational frequency to maximum phonon frequency while the radiative relaxation rate should increase as the cube of the vibrational frequency. Because of this, a long relaxation time window could occur in the 10  $\mu\text{m}$  wavelength region [6.41].

High resolution diode laser spectroscopy and the nonequilibrium techniques of laser saturation and transient hole burning spectroscopy over a wide temperature range can be used to identify the microscopic mechanisms responsible for  $T_1$  (the energy relaxation time) and  $T_2$  (the dephasing time) in various alkali halides [6.42]- [6.46] . The intrinsic symmetry and simplicity of this hole-burning system have allowed many features of the anharmonic decay process to be identified: the decay channel consists of multistep emission of lower-energy internal modes, localized modes, and band phonon modes [6.46]. It was in the course of these transient hole burning measurements, that the production of persistent spectral holes at extremely low laser powers was first observed in a vibrational mode in a crystal lattice [6.9].

#### 6.1.2 Persistent IR hole burning in vibrational modes

The three major sections in this chapter describe in turn three examples of persistent vibrational mode hole burning. This division is natural because the spectra for the three molecule-host systems are strikingly different although the underlying process appears to involve molecule reorientation in each case. The description of the salient features of these systems should provide a framework for the interpretation of future studies of vibrational modes in solids showing PIRSH formation.

In the next section the persistent properties of the molecule 1,2-difluorethane (DFE) in van der Waals matrices are described. At low burning powers such as those available from Pb-salt semiconductor diode lasers, the  $\nu_{17}$  mode of the trans conformation of  $\text{CH}_2\text{F}-\text{CH}_2\text{F}$  matrix-isolated in Ar, Kr or  $\text{N}_2$  shows PIRSHs due to molecular reorientation in the host. At the higher laser powers available from  $\text{CO}_2$  lasers, however, a different hole-burning mechanism becomes observable: conformer interconversion.

Section 6.3 is devoted to a discussion of the persistent spectral hole dynamics of the  $\nu_3$  vibrational mode of tetrahedral  $\text{ReO}_4^-$  molecules substitutionally doped into alkali halide single crystals. The holes and antiholes are produced with  $10.8\text{ }\mu\text{m}$  radiation from  $\text{CO}_2$  and semiconductor diode lasers also at intensities far below saturation intensity levels. The PIRSH mechanism is photon-induced  $90^\circ$  reorientation of the molecule in the crystal cage. This defect-lattice system also has the distinction of proving that PIRSH's can occur in infrared-active impurity modes in crystalline hosts.

For the  $\text{CN}^-$  molecule in alkali halides, a molecular reorientation of  $180^\circ$  occurs during PIRSH formation but the low symmetry of the molecule and the proximity of a second dopant yield hole burning properties quite different from the  $\text{ReO}_4^-$ -alkali halide system. These results are described in Sec. 6.4. Current research is uncovering even more vibrational mode-lattice systems that show PIRSH production without requiring transitions among TLS's or other degrees of freedom associated with the host lattice.

## 6.2 Molecules in van der Waals matrices

### 6.2.1 1,2-Difluoroethane

#### 6.2.1.1 Diode laser measurements

IR hole burning with a low intensity (  $10 \text{ mW/cm}^2$  ) tunable diode laser has been demonstrated for one of the matrix-split components of the  $\nu_{17}$  mode of the *trans* conformation of  $\text{CH}_2\text{F}-\text{CH}_2\text{F}$  matrix-isolated in Ar [6.6]- [6.8] or Kr [6.7] - [6.8] and both of the components in  $\text{N}_2$  [6.8]. These investigations have attracted widespread interest because this ultrahigh resolution probe, if applicable to matrix-isolated molecules in general, would provide an analytical tool of considerable power. The central issue which was addressed with these first sets of measurements is the identification of the mechanism behind the persistent spectral effects. The experimental results which are reviewed here indicate that molecular reorientation in the matrix cage during vibrational de-excitation is the most likely cause of the low intensity hole burning effect.

##### 6.2.1.1.1 $\text{CH}_2\text{F}-\text{CH}_2\text{F} : \text{Ar}$

Upon deposition of 1,2-difluoroethane (DFE) in Ar (  $M/A = 1000$  ) from room temperature onto a 17 K cold plate approximately 20 % of the molecules remain trapped in the less stable *trans* form [6.47]. The dashed trace in Fig. 6.2 shows one of the matrix split components of the inhomogeneously broadened  $\nu_{17}$  absorption band of the *trans* conformation in Ar at 4.6 K which is centered at  $1047.54 \text{ cm}^{-1}$  with a linewidth of  $0.17 \text{ cm}^{-1}$ . (The other two components are centered at  $1049.5 \text{ cm}^{-1}$  and  $1045.6 \text{ cm}^{-1}$ , respectively.) The solid trace shows the same feature with a spectral hole burned in it at  $1047.46 \text{ cm}^{-1}$  [6.8]. By shifting

the diode frequency a hole can be produced in a few minutes at any position in this band. The hallmark of this process is that for fixed laser frequency the transmittance of the sample is observed to increase as a function of time, rapidly at first and then finally approaching a limiting value at longer times. After the burn is completed, the laser intensity is attenuated and the frequency swept continuously to produce a spectrum such as that represented by the solid trace in Fig. 6.2. The difference between the two traces identifies both the hole and antihole positions. Note that the antihole is broader than the hole and its frequency position is between that of the hole and band center. This result is obtained independent of where the hole is placed. An experimental reason accounts for the difference in area between the hole and antihole shown in Fig. 6.2: even with the laser attenuated some additional burning occurs during the frequency sweep. Thus the key experimental finding which will help in the identification of the underlying mechanism is that the integrated area of this band does not change after hole burning.

An experimental problem has been that the hole strength at low temperature decays with time with a decay constant which depends on the radiation shielding in the cryostat. When the optical access ports are blocked by the 50 K shield which surrounds most of the sample, the decay constant decreases by an order of magnitude [6.8]. Keeping this difficulty in mind an estimate of the low temperature quantum efficiency of the hole burning process,  $\eta$ , (defined as number of molecules burned / number of absorbed laser photons ) can be obtained. For the Ar host the measured value is quite large:  $\eta = 0.03$ . With increasing sample temperature above 10 K the decay constant increases rapidly due to a thermal deactivation process so that by 17 K the decay is so fast that hole burning is no longer detectable.

From the width of the low temperature hole an estimate can be obtained for the relaxation time of the excited vibrational state [6.8]. For short irradiation times a Lorentzian line shape

is observed. In this limit the measured width of the hole is twice the homogeneous line width. By extrapolation the measured width at 0 K is obtained and identified with the vibrational relaxation time,  $T_1$ , under the assumption that the dephasing is dominated by excited state decay. For the Ar matrix the estimate for  $T_1 = 3.5$  nsec.

Hole burning has been attempted on the other strong matrix split component (with no effect [6.48]) and also on several bands of the *gauche* and *trans* conformation which were brought into coincidence with the laser modes by using fully deuterated DFE. None of the four deuterated bands investigated ( *trans* ( $980\text{ cm}^{-1}$ ) nor *gauche* ( $974\text{ cm}^{-1}$ ,  $989\text{ cm}^{-1}$ , and  $1239\text{ cm}^{-1}$ ) ) showed any signs of hole burning.

#### 6.2.1.1.2 $\text{CH}_2\text{F}-\text{CH}_2\text{F} : \text{Kr}$

The hole burning results on one of the matrix split  $\nu_{17}$  mode absorption lines ( $1050.4\text{ cm}^{-1}$ ) for the Kr host are similar to those obtained with Ar except the holes are more stable. By shielding the sample completely from room temperature background radiation the lifetime of the holes at liquid helium temperatures is measured to be about 24 hours [6.7]. With the optical access ports open the lifetime is reduced by an order of magnitude. For this system  $\eta = 0.01$ .

The thermal deactivation process becomes important at temperatures greater than 15 K and the holes erase rapidly at 28 K. Nevertheless, the hole profile can be measured up to 22 K. The temperature dependence of the homogeneous line width for short irradiation times is shown in Fig. 6.3. The observed width is independent of the laser frequency in the band. Note that the laser line width is about an order of magnitude smaller than the smallest width shown in Fig. 6.3. To interpret these results the authors assume that the temperature dependence of

the line width comes from dephasing ( $T_2$ ) processes which vanish as  $T \rightarrow 0$ . The three curves superimposed on top of the data in Fig. 6.3 are for the Raman dephasing process associated with phonon scattering. For the Debye model, the solid curve is for a best fit with  $\theta_D = 38$  K and the dashed curve for  $\theta_D$  (Kr) = 72 K. The dotted curve describes a similar process but for a local mode (Einstein oscillator) centered at  $\theta_E = 38$  K. The homogeneous width at  $T = 0$  gives  $T_1 = 4.3$  nsec.

Burning and analyzing the hole strength with polarized radiation demonstrates that the molecules are not freely rotating at low temperature. The experimental data are shown in Fig. 6.4 with the spectrum of the virgin sample displayed at the top. The notations V and H denote vertical and horizontal polarization directions for either the burn or probe beams. The hole intensity ratio for perpendicular and parallel polarization directions is found to be 1/3. If the molecules are rotating with a period small compared to the measuring time (a few minutes) then no difference in hole strength between the two polarizations in a given trace should occur in disagreement with the experiment.

#### 6.2.1.1.3 $\text{CH}_2\text{F}-\text{CH}_2\text{F} : \text{N}_2$

In the diatomic matrix  $\text{N}_2$ , the  $\nu_{17}$  mode of DFE is split by the matrix into two components, a strong band labeled A at  $1045.39 \text{ cm}^{-1}$  and a weaker band, B, at  $1046.17 \text{ cm}^{-1}$ . Fortunately, both bands are covered by two adjacent diode laser modes[6.8]. Hole burning can be seen in either of these bands and in addition the antihole or product state from each appears spread over a new inhomogeneously broadened band, C, centered at  $1046.21 \text{ cm}^{-1}$  which is resolved from band B. This redistribution of oscillator strength into a frequency region separated from the original inhomogeneously broadened band is very different from that found for the other two matrices; in addition, once band C is populated, then sharp holes can be



burned in it as well. The  $T \rightarrow 0$  vibrational relaxation time is comparable to that observed for the other two hosts, namely,  $T_1 = 2.2$  nsec. The temperature dependence of the erasing of the holes is about the same as that found in the Ar host.

#### 6.2.1.2 $\text{CO}_2$ laser measurements

##### 6.2.1.2.1 Molecular monomers

Site conversion for the *trans*  $\nu_{17}$  doublet for DFE :  $\text{N}_2$  was first observed by *Frei et al.*[6.49] with a moderate intensity cw  $\text{CO}_2$  laser. Because of the displacement of band C from B or A, the pump could be a fixed frequency laser and the probe beam, a high resolution spectrometer. This experimental technique with cw  $\text{CO}_2$  laser intensities  $10^4$  times larger than earlier diode values was used to probe  $\text{CH}_2\text{F}-\text{CH}_2\text{F}$  isolated in Ar, Kr and Xe in the high intensity regime [6.50].

Due to the accidental coincidence of the  $\text{CO}_2$  laser lines 9R(6) and 9R(8) with the  $\nu_{16}$  doublet band of *gauche*  $\text{CH}_2\text{F}-\text{CH}_2\text{F}$  : Ar, earlier measurements already have produced a negative result [6.49] for PIRSH production. Unfortunately, the  $\nu_{17}$  triplet (1049.5, 1047.6, and  $1045.6 \text{ cm}^{-1}$ ) associated with monomeric *trans* DFE in Ar is not coincident with any  $\text{CO}_2$  laser line. In addition, irradiation of the sample for several hours with unfiltered radiation from a glowbar source produced no spectral changes in band strengths so this host-defect system will be set aside temporarily.

IR irradiation of  $\text{CH}_2\text{F}-\text{CH}_2\text{F}$  in Kr and Xe hosts gives positive results: radiation coincident with the  $\nu_{17}$  absorption of *trans* DFE induces a frequency selective *trans*  $\rightarrow$  *gauche* conversion. Since the experimental results are similar for both defect-host systems only the

DFE : Xe results will be outlined here [6.50]. Figure 6.5 shows the IR spectra of *trans* and *gauche* DFE : Xe in the region of the C-F stretch modes for different conditions of irradiation after the sample had been fabricated in the dark. Figure 6.5b displays the labelling of the different bands, two of which are coincident with CO<sub>2</sub> laser lines. The  $\nu_{16}$  mode of *gauche* DFE is matrix split into two lines near 1062 cm<sup>-1</sup> which overlap the 9P(4) laser line and the  $\nu_{17}$  mode of *trans* DFE is split into three components near 1045 cm<sup>-1</sup> which overlap with the 9P(22) line. The laser frequencies are identified in Fig. 6.5c.

The solid line in Fig. 6.5a shows the line strengths as measured with a filtered glowbar source immediately after the matrix was deposited in the dark. The dashed trace in the same figure indicates how the strengths have changed after the sample had been exposed to unfiltered IR source radiation for 1.5 hrs. Clearly, the IR radiation facilitates the conversion of the more stable *gauche* to the less stable *trans* DFE. Figure 6.5b shows the spectrum for a sample in a photostationary state. It had been illuminated both during deposition and also for the next 2 hrs with unfiltered glowbar light. Changing to the filtered source induces a slow back-conversion from *trans* to *gauche* DFE. The effect of the 9P(22) laser light on this conversion is shown in Fig. 6.5c. The dashed trace identifies the initial state and the solid trace, the spectrum after 100 min. of laser illumination at an intensity of 130 mW/cm<sup>2</sup>. A dramatic decrease in the strength of the lower frequency *trans* site is observed; in addition, the laser-induced production of *gauche* DFE appears in the higher frequency component of the  $\nu_{16}$  absorption doublet. A similar irradiation procedure with 9P(4) in the *gauche* band does not cause hole burning, *gauche*  $\rightarrow$  *trans* conversion or any other change whatsoever in the spectrum.

A close examination of the *trans* region with a spectrometer resolution of 0.4 cm<sup>-1</sup> (FWHM) at intermediate laser illumination times shows that persistent hole burning exists at the laser frequency. The hole depth, as determined by this low resolution probe beam, is 50 % after

irradiation for a 30 min interval. This observation demonstrates that a frequency selective *trans*  $\rightarrow$  *gauche* conversion is taking place.

#### 6.2.1.2.2 Molecular aggregates in Ar

When the molecular concentration in Ar is increased so that  $M/A = 850$  then the three site components of the  $\nu_{17}$  mode of *trans* DFE are superimposed on top of a broad background feature [6.51]. Irradiated of this feature with 9P(18) light induces persistent hole burning which can be detected with an IR spectrometer with a resolution of  $0.25 \text{ cm}^{-1}$  after laser illumination for 10 min with an intensity of  $750 \text{ mW/cm}^2$ . After exposure to unfiltered source light for 30 min. the hole is erased and the band recovers its original shape.

New broad absorption features appear when the concentration is increased to  $M/A = 90$ . Hole burning can now be identified in both the *gauche* and *trans* absorption bands as well as in a new aggregate band which appears at  $1060 \text{ cm}^{-1}$ , but no evidence of conformational interconversion between *gauche* and *trans* is observed. Again the presence of unfiltered source light erases the holes in about 30 min. [6.51].

#### 6.2.2 Interpretation of persistence

The low intensity diode and high intensity  $\text{CO}_2$  laser measurements probe two different regimes of hole burning in matrix-isolated DFE. For low intensities the main findings are as follows: (1) spectral persistence is produced by a one photon process, (2) the low concentrations insure that the process involves a single molecule, (3) for the Ar and Kr matrices the matrix-split modes do not show the same hole burning behavior, (4) the hole polarization property demonstrates that the molecule is not rotating freely nor tunneling

rapidly around a fixed site, (5) for the Ar and Kr matrices the antihole (product state) remains within the inhomogeneous line while for the N<sub>2</sub> matrix the oscillator strength is transferred among three different inhomogeneous lines, and (6) the erasing of the hole by room temperature thermal radiation and by modest temperature cycling indicates that the process contains a thermal activation energy and is reversible.

The measurements on DFE:Kr and DFE:Xe with a CO<sub>2</sub> laser in conjunction with a thermal global source provide the following additional results: (7) unfiltered source radiation induces a *gauche*  $\leftrightarrow$  *trans* conversion, (8) laser radiation coincident with the  $\nu_{17}$  mode of *trans* DFE induces hole burning and a *trans*  $\rightarrow$  *gauche* conversion, (9) laser radiation coincident with the  $\nu_{16}$  mode of *gauche* DFE induces no change, (10) filtered source radiation (  $< 1450\text{ cm}^{-1}$  transmitted ) induces a very slow *trans*  $\rightarrow$  *gauche* conversion, and (11) the thermal source radiation induces no change in the spectrum of DFE:Ar (excluding for the moment the single aggregate study).

Three fundamentally different kinds of vibrationally induced structural rearrangements all could be sources of the observed persistent spectral changes for this matrix-isolated molecule. The first type (photochemical) involves the shape change of the molecule itself (the *trans* - *gauche* conversion), the second (photophysical) involving rearrangement of the neighboring matrix, and the third (photophysical) involving reorientation of the rigid molecule in the matrix.

Items (7) through (10) listed above definitely show that photochemical conversion is taking place, and the frequency selectivity mentioned in item (8) illustrates that the effect is not produced by local heating. Item (11), on the other hand, demonstrates that the photochemical rate is dependent on the host in a crucial way. There is additional evidence

from the low intensity work that photochemical conversion is not the sole mechanism behind the observed hole burning.

At low intensity the oscillator strength of the inhomogeneously broadened  $\nu_{17}$  mode in *trans* DFE:Kr is independent of the burning (item (5)) in marked contrast with the high intensity results. This behavior is consistent with a photophysical process involving motion of the molecule and/or rearrangement of the local lattice. *Dubs et al.* [6.8] have carried out model calculations with the DFE molecule in a substitutional site in an fcc lattice and conclude that the photophysical hole burning is caused by a reorientation of the molecule across a large barrier to an energy configuration which would be equivalent except for the occurrence of nearby lattice defects. The nonspherical shape of the  $N_2$  host molecule eliminates the orientational degeneracy of DFE so that the inequivalent directions which are still connected by a large energy barrier have vibrational transition energies separated by more than the inhomogeneous linewidths. Presumably the photophysical hole burning for the DFE aggregates in Ar is produced by a similar process.

It is possible to distinguish both photophysical and photochemical hole burning with excitation of the same vibrational mode for Kr isolated DFE because the efficiencies for the two processes are very different: for the photophysical process the efficiency  $\eta \approx 10^{-2}$  while for the photochemical hole burning  $\eta \approx 10^{-6}$ . The  $\nu_{17}$  mode of *trans* DFE in Kr is characterized by a very complex matrix-split spectrum with six absorption lines at  $1051.4 \text{ cm}^{-1}$ ,  $1050.4 \text{ cm}^{-1}$ ,  $1048.5 \text{ cm}^{-1}$ ,  $1046.9 \text{ cm}^{-1}$ ,  $1045.0 \text{ cm}^{-1}$ , and  $1042.9 \text{ cm}^{-1}$ , respectively but so far diode laser measurements have been reported only for the  $1050.4 \text{ cm}^{-1}$  transition. A continued exploration of DFE in this host is to be encouraged. Probing the sample simultaneously with the diode and one of the four coincident  $CO_2$  laser lines is an approach which would enable one to examine with some precision the interplay between these different processes.

### 6.2.3 Molecular aggregates of methyl nitrite or methanol

Methyl nitrite (MEN) has been studied [6.50] at a relatively high concentration ( $M/A = 300$ ) in a nitrogen matrix with a nominal layer thickness of  $25\ \mu\text{m}$ . The experimental procedure is first to record the spectral region (about  $15\ \text{cm}^{-1}$ ) around the  $\nu_7$  *trans* band ( $\text{FWHM} = 2.8\ \text{cm}^{-1}$ ) then to irradiate the sample with  $170\ \text{mW}/\text{cm}^2$  of cw  $\text{CO}_2$  laser radiation at 9P(28) for about 10 min and, finally, to block the laser beam and record the spectral region a second time. A spectral hole is observed in the second scan at the laser frequency with a depth that decays with time. This decay time increases when an IR band pass filter is placed in front of the sample indicating that the broad band thermal radiation from the source erases the hole. From the hole width a lower limit of 100 psec is estimated for the vibrational relaxation time from the excited state. The line shapes of other vibrational absorption bands of *trans*  $\text{MEN:N}_2$  at different frequencies are found to be independent of this hole burning at 9P(28). The location of the displaced oscillator strength has not been identified.

Analogous measurements [6.50] on *trans*  $\text{MEN:Ar}$  show the same behavior at the laser frequencies 9P(28) and 9P(26) but not at 9P(24). Since the monomer component has a peak at this last frequency, the persistence does not appear to be associated with isolated molecules but instead with dimers, trimers, etc.

Methanol in an argon matrix ( $M/A = 200$ ), layer thickness,  $20\ \mu\text{m}$ , also shows persistent hole burning in the C - O stretch vibrational mode region [6.50]. Laser irradiation with 9P(38) or 9P(40) in the broad band associated with methanol dimers generates holes but no holes are produced when the frequency is tuned to the strong band produced by isolated methanol or the transitions due to other aggregates. These results indicate that although some degree of

molecular complexity is important, aggregation, in general, can not be relied upon to guarantee persistent spectral effects.

*Felder and Günthard* [6.50] have speculated on the possible causes of these persistent effects. They eliminate the *trans*  $\rightarrow$  *cis* isomerization of  $\text{MEN} : \text{Ar}, \text{N}_2$  as a possibility because of the large barrier between the two conformers. In addition, one would expect that if a photon assisted conformation had occurred then holes should have appeared in many of the normal mode bands of the complex but the experiments show that a hole only appears at the burn frequency. They propose that the inhomogeneously broadened bands are produced by the many geometric arrangements available to the aggregates and that the persistence stems from the laser-induced rearrangement of those resonant complexes which happen to coincide with the driving frequency. Although the model is plausible, it is unlikely that only one normal mode would be changed after such a collective rearrangement. A precise measurement of the difference in band shapes before and after irradiation should be made to pinpoint how the oscillator band shapes and strengths are altered.

### 6.3 $\text{ReO}_4^-$ in Alkali Halide Crystals

#### 6.3.1 Background and spectroscopic information

In this section we describe the persistent spectral hole dynamics for a high-symmetry photostable molecule in several crystalline alkali halide hosts. The  $\text{ReO}_4^-$  molecule (perrhenate ion) was originally selected for study because one of the four vibrational modes of this tetrahedral molecule, the  $\nu_3$  mode, lies in the wavelength range spanned by the  $\text{CO}_2$  laser (9-10  $\mu\text{m}$ ). The molecule is stable at the temperatures required for the growth of alkali halide crystals and enters the crystal substitutionally in appreciable concentrations for those crystals with lattice constants larger than that of NaCl. Because the molecule has a much larger ionic radius than the halogen ions for which it substitutes, rotational motion is suppressed and steric effects are important. There are only two distinct symmetry-preserving orientations of the tetrahedral molecule in the octahedral anion site. Thus, perrhenate ions in alkali halides are ideally suited for spectroscopic study of a zero-phonon vibrational transition at low temperatures.

Before tunable semiconductor diode lasers in the infrared became available, a major experimental problem was to produce a coincidence between the fixed frequency  $\text{CO}_2$  laser lines and the  $\nu_3$  mode at liquid helium temperatures. The experimental difficulty is illustrated in Figure 6.6 which shows a diode laser trace in the 10 $\mu\text{m}$  wavelength region of the transmissivity of both a sample of  $\text{ReO}_4^-$  molecules in KI at low temperatures and a hot  $\text{CO}_2$  gas cell[6.43]. The vibrational absorption line can be as narrow as  $0.016\text{ cm}^{-1}$  at 1.4K[6.43]. With this type of measurement the frequency interval between the nearest  $\text{CO}_2$  laser line and the  $\nu_3$  mode can be determined. Inspection of this figure shows that the two frequencies do



not coincide and that the chance of an accidental coincidence between the comb of  $\text{CO}_2$  laser lines (spaced almost  $2 \text{ cm}^{-1}$  apart) and the vibrational mode absorption is very small.

One way to circumvent this problem is to use "poor man tuning", or double-doping, to intentionally induce excess inhomogeneous broadening of the zero-phonon line. This broadening is accomplished by adding a second cation dopant to the melt [6.42], [6.52] when the crystal is grown. The second impurity, depending on its position in the lattice, inhomogeneously strain broadens or splits the  $\nu_3$  absorption line producing an overall linewidth on the order of  $1\text{-}2 \text{ cm}^{-1}$ . Line coincidences can also be produced simply by hot-forging the  $\text{ReO}_4^-$  doped alkali halide sample before cooldown[6.11]. With either method of sample preparation it becomes relatively easy to find a  $\text{CO}_2$  laser line coincidence with some part of the  $\nu_3$  absorption spectrum and therefore perform saturation and hole-burning measurements.

### 6.3.2 Measurements of relaxation times $T_1$ and $T_2$

The relaxation dynamics of the  $\nu_3$  mode provide an important framework for the interpretation of persistent spectral hole-burning results. The excited state relaxation time  $T_1$  and the dephasing time  $T_2$  have been measured at low temperatures for perrhenate ions in alkali halides by a combination of spectroscopic techniques[6.44]- [6.46] , including incoherent laser saturation and transient hole-burning spectroscopy.

Incoherent laser saturation studies of the  $\nu_3$  mode absorption at two different temperatures are illustrated in Figure 6.7. The room temperature data follow the shape expected for a homogeneously broadened system while the 1.4 K data agree with the shape expected for an inhomogeneously broadened system. In the first case the saturation intensity,  $I_s$ , is directly related to the energy relaxation time  $T_1$  through the usual relation

$$I_s = \frac{h\nu}{2\sigma T_1} \quad (6.1)$$

where  $\nu$  is the vibrational mode frequency, and  $\sigma$  is the absorption cross section. In the low-temperature case,  $I_s$  is directly related to the product of  $T_1$   $T_2$  through

$$I_s = \frac{n\hbar^2}{8\pi T_1 T_2 L(|\tilde{\mu}|^2/3)}, \quad (6.2)$$

where  $n$  is the index of refraction,  $L$  is the local field factor, and  $\tilde{\mu}$  is the dipole moment of the transition. In this second case  $T_2$  can be obtained independently from transient (two-level) hole-burning spectroscopy since the hole width is directly connected to the homogeneous linewidth through the relation  $\Delta\nu_{\text{hole}} = (2/\pi T_2) = 2\Delta\nu_{\text{hom}}$  (in the absence of spectral diffusion effects).

Using Eqs. (6.1) and (6.2), values of  $T_1$  and  $T_2$  have been determined for the  $\text{ReO}_4^- \nu_3$  mode in a variety of alkali halide hosts [6.45] [6.46]. Table 6.1 shows the results of these measurements. Within experimental error,  $T_2$  is approximately equal to  $2T_1$  indicating that the  $\nu_3$  mode is lifetime broadened at liquid helium temperatures. Thus, in this case  $I_s$  is proportional to  $(T_1)^{-2}$ . Since  $(1/T_1)$  is a measure of the excited state decay rate, then according to the simple energy gap law [6.40], a plot of  $\log I_s$  versus  $\nu_3/\nu_{\text{lattice}}$  where  $\nu_{\text{lattice}}$  is a dominant lattice phonon frequency should produce points that lie on various straight lines with each line corresponding to a different alkali or halide series.

Figure 6.8 shows one plot of such data. The ratio of the  $\nu_3$  frequency to the maximum frequency in the longitudinal acoustic spectrum (the number of LA phonons required to relax the  $\nu_3$  mode) is plotted along the abscissa. Since for the assumed multiphonon decay

mechanism the data for NaI, KI and RbI should lie on one straight line while the data for RbCl, RbBr, and RbI should line on another, one can conclude that the actual decay scheme must be more intricate than simple multiphonon decay. A systematic study of these data suggests that the low temperature decay channel actually consists of multistep emission of other internal molecular modes, localized phonon modes, and band phonons[6.46]. Although this decay scheme is more complex, it is also more probable because it is of lower order than simple multiphonon decay. Further, this lower-order decay scheme also accounts for the relatively small value of  $T_1$  ( $\approx 10^{-8}$  s) and the large value of  $I_s$  ( $1-10 \text{ W/cm}^2$ ) at low temperatures.

### 6.3.3 Persistent spectral holes for $\text{ReO}_4^-$ in alkali halides

#### 6.3.3.1 Summary of characteristics

By far, the most interesting part of Fig. 6.7 is the persistent change in sample transmission which appears at very small laser intensities. This is due to the formation of persistent spectral holes under the action of the incident laser light. The holes were produced with  $10.8 \mu\text{m}$  radiation from  $\text{CO}_2$  and semiconductor diode lasers at intensities far below the two-level saturation intensity,  $I_s$ . The hole formation in this system appears to involve reorientation of the excited impurity molecule during nonradiative vibrational de-excitation. These holes have a variety of novel properties, and a brief description of the hole dynamics forms the remainder of this section. (For more detail, the reader is referred to Ref. [6.10].) As a result of these measurements, persistent nonphotochemical hole-burning at low laser intensity is shown to be a general solid-state phenomenon which may be reasonably expected to occur whenever the complete ground state of the system has configurational degeneracy.

Figure 6.9 shows the growth and detection of a persistent spectral hole in  $\text{RbI}:\text{ReO}_4^-$  using a single  $\text{CO}_2$  laser (called the probe). The fixed frequency probe laser burns a hole, and time-varying probe laser transmission serves as a measure of hole depth. After cooling the sample to 1.4K in the dark, the laser is unblocked at time  $t_1$  (Fig. 6.9a). The vertical axis in Fig. 6.9 shows the infrared power transmitted through the sample as a function of time. The initial sample transmission is  $T_i$ ; it then slowly grows over many seconds to a steady-state value  $T_{ss}$ . If the laser is now blocked for a period of, say, 10 minutes and then unblocked the sample transmission is observed to remain at the larger  $T_{ss}$  value indicating that the spectral hole has not decayed away.

One way to erase the hole is to use a second  $\text{CO}_2$  laser which is set roughly 10 MHz away from the first one. When this second laser irradiates the sample from  $t_2$  to  $t_3$ , as shown in Fig. 6.5b, then the hole burned by the first laser is erased. If the second laser is turned off then the transmission again rises to  $T_{ss}$  signifying reburning of the first hole. This is a general phenomenon: laser light in the wings of a previously burned hole cause hole erasure, signifying that the product absorption for the initial hole is only slightly displaced from the initial state absorption. Another way to erase the hole is to simply cycle the sample temperature up to 20 degrees K and back down. Thus the spectral holes in this system only have long lifetimes at temperatures less than 10 K.

To measure the hole lineshape, either a tunable diode laser or a second cavity-length tuned  $\text{CO}_2$  laser can be utilized to scan the hole directly. Figure 6.10 shows the hole lineshape as determined by the latter technique. The hole spectrum consists of a single, central hole of width  $10 \pm 2$  MHz in RbI and  $20 \pm 4$  MHz in KI, which is essentially identical to the hole lineshape for transient saturation holes [6.44]. The hole width is independent of temperature below 10K, and grows very quickly above 10K. In addition, the hole depth

$\Delta\alpha/\alpha_i \equiv (\alpha_i - \alpha_f)/\alpha_i$  appears to saturate at a shallow value in the range from 0.05 to 0.3 independent of the burning laser power.

Curves like those presented in Fig. 6.9 also illustrate the kinetics of hole growth for the  $\text{ReO}_4^-$  - alkali halide systems. The hole growth is nonexponential, showing a fast rate at small burning time and slower and slower rate as hole-burning continues. Nevertheless, an effective quantum efficiency at  $t = 0$ ,  $\eta_e$ , can be determined from the data to be roughly equal to  $10^{-3}$ . Values in this range are typical of the  $\text{ReO}_4^-$  system, and are to be contrasted with the  $10^{-5}$  to  $10^{-7}$  efficiencies that have been reported for NPHB in electronic transitions (see Chapter 5).

Since the inhomogeneously broadened  $\nu_3$  mode absorption is  $1\text{-}2\text{ cm}^{-1}$  in width in the RbI and KI hosts, attempts were made with a tunable diode laser to burn holes at frequencies other than the 10P(42)  $\text{CO}_2$  laser line at  $10.8\text{ }\mu\text{m}$ . The 10P(42) laser line is  $\approx 2.2\text{ cm}^{-1}$  from the  $^{187}\text{ReO}_4^-$  line center in RbI, and  $0.22\text{ cm}^{-1}$  from the  $^{187}\text{ReO}_4^-$  line center in the KI hosts. Detectable persistent holes could not be burned with the diode laser in the immediate region of the  $\nu_3$  mode line center in either KI+0.001 mole %  $\text{KReO}_4$  or RbI+0.001 mole %  $\text{RbReO}_4$ . These results suggest that the long-lived hole-burning phenomenon is somehow associated with the larger values of strain found in the wings of the inhomogeneously broadened line.

### 6.3.3.2 Model for the PIRSH process

A natural configuration for the  $\text{ReO}_4^-$  molecule substituted for the halide ion in an alkali halide crystal is with the four tetrahedral Re-O bonds directed along four of the eight available  $\langle 111 \rangle$  directions. Indeed, careful studies of the infrared and Raman spectra of  $\text{ReO}_4^-$

molecules in alkali halides [6.53] indicate that the symmetry of the  $\text{ReO}_4^-$  molecule in the solid is still tetrahedral to high accuracy. Examination of an ionic model for the lattice with the  $\text{ReO}_4^-$  at the halide ion site shows that the steric pressure from nearby ions is somewhat relieved if the Re-O bonds lie along  $\langle 111 \rangle$  body diagonals.

The molecular ion thus may be expected to have two configurations in the lattice related by a  $\pi/2$  rotation about a  $\langle 100 \rangle$  axis with a high barrier to rotation between the two configurations. Infrared spectroscopy of the  $\nu_3$  mode absorption (over a range of several  $\text{cm}^{-1}$ ) [6.10] suggests that there are no strong librational absorptions at low temperatures, in contrast to the situation for  $\text{CN}^-$  molecules in alkali halides [6.58], for instance.

The most reasonable first model for the persistent hole formation mechanism involves a photostimulated reorientation of the molecule between these two normally equivalent orientations. The model that originally evolved out of the early work was very similar to that used by *Hayes et al.* [6.1] to explain NPHB in glasses in the visible. The principal difference was that in the infrared case, the configurational degeneracy is not provided by the presence of the nearby tunneling systems in the host matrix, but rather by the two possible orientations of the molecule in the crystalline host.

Two possible vibrational deexcitation pathways of the  $\nu_3$  mode which can give rise to optically induced reorientation are indicated in Figure 6.11. Pathway P1 is that proposed previously for the glasses; photoexcitation in well A and configurational tunneling to the new configuration B while in the optically excited state, with subsequent relaxation to the ground state of this second configuration. The alternative pathway is P2, photoexcitation in configuration A, return to an excited librational state within well A, subsequent tunneling in this librational state to well B and finally relaxation to the new ground state. The consequence

of the resultant molecular reorientation is to shift the absorption at any particular active site from the frequency corresponding to a vertical transition between wells in configuration A to a different frequency corresponding to a vertical transition between wells in configuration B. Because there is a distribution of both A and B sites, molecules which initially have vibrational frequencies coincident with the laser frequency end up being reoriented to the alternate configuration which absorbs at a slightly different energy so that a spectral hole results.

Using the level structure in Fig. 6.11, a phenomenological rate equation model can be developed that can be used to compute the hole growth characteristic and the hole lineshape[6.10]. Although the model predicts the correct experimental behavior in most regimes, a fundamental problem has been that it also predicts librational states in the far infrared absorption spectrum of the material, yet none have been observed. This mystery has been resolved with the discovery of the antihole, or "peg".

#### 6.3.4 Persistent spectral pegs

Figure 6.12 shows a transmission spectrum of a thick alloy sample ( $\text{KI} + 0.05 \text{ mole } \% \text{ KReO}_4 + 2 \text{ mole } \% \text{ NaI}$ ) at 6K as measured with a high resolution Fourier transform spectrometer. The doublet structure of the  $\nu_3$  mode comes from the two Re isotopes. The two doublets farthest removed from the unperturbed mode at  $923.5 \text{ cm}^{-1}$  appear because of a nearby  $\text{Na}^+$  impurity. The close-in doublets come from  $\text{Na}^+$  impurities further away from the  $\text{ReO}_4^-$  ion. The laser coincidences for both  $\text{N}_2\text{O}$  and  $\text{CO}_2$  lasers for all perturbed  $\nu_3$  frequencies are also indicated in Fig. 6.12. The important observation is that now a number of laser transitions are coincident with vibrational modes of the perturbed and unperturbed ionic absorptions.

The persistent holes which have been burnt using  $\text{N}_2\text{O}$ , P(19) are very similar in behavior to those produced by  $\text{CO}_2$ , 10P(42) in the main band. The surprising result is that at the P(17) line of  $\text{N}_2$ , a persistent antihole (peg) is produced[6.11].

An enlargement of the important spectral region is shown in Figure 6.13a. A first derivative spectroscopic measurement of the peg has been made with a tunable low power diode laser in Figure 6.13b. The line shape corresponds to a central line of enhanced absorption with a full width at half maximum of 28 MHz, but surrounded by broad wings of decreased absorption. The overall shape is a negative replica of the persistent hole which had been observed at the  $10.8\text{ }\mu\text{m}$  P(42)  $\text{CO}_2$  line. A reexamination of other  $\text{ReO}_4^-$ -host lattice combinations at a number of  $\text{N}_2\text{O}$  frequencies has shown that this peg formation phenomenon is quite general. Persistent holes or persistent pegs occur depending upon the particular spectral position and the particular sideband in which irradiation occurs.

By now one should be intuitively comfortable with the idea that narrow-band laser radiation within an inhomogeneously broadened absorption line might lead to a burned spectral hole through saturation, photodecomposition, photoinduced reorientation or perhaps other processes which remove absorbers from the spectral region under irradiation. An increased absorption at the frequency of irradiation is not so easy to explain. A simple but subtle variation in the model described earlier (Fig. 6.11) appears to account qualitatively for the persistent hole and peg phenomena. Once again we imagine that the local lattice strain gradients make the two ground state orientations, A and B, of the tetrahedral molecule in the cubic site inequivalent (see Fig. 6.14). In addition it is assumed that the energies of the two orientations in the excited vibrational states A' and B' are different from the ground state. Although the random nature of the strain field produces distributions of all of these energy levels, the important features with respect to hole and peg production can be demonstrated



with the four levels shown in Fig. 6.14. In arrangement (1) the potential-well asymmetry in the ground state is larger than the asymmetry in the excited state while the converse is true for arrangement (2). For both cases, well asymmetry is assumed to be large compared to the tunnel splitting so the infrared selection rule strongly favors left well-left well or right well-right well transitions. These transitions are labeled AA' and BB' in the lower part of the figure. The nearly forbidden transitions between configurations, labeled AB' and BA', are the pathways that lead to persistent elastic polarization of the resonant molecules.

When the laser frequency  $\omega_p$  is not symmetrically located with respect the AA' and BB' transition frequencies in Fig. 6.14, persistent spectral effects are produced. For the energy level arrangement (1) the laser pump drives centers from A to B via the overlap of the laser with the homogeneous width of the AB' transition. Since the number in A decreases, the strength of AA' decreases and a hole appears at the pump frequency. For the energy level arrangement (2) the laser pump again drives centers from A and B via the AB' transition but increased absorption now occurs near  $\omega_p$  since the dominant absorption results from the overlap of the homogeneous width of the BB' transition with the laser line instead of the AA' transition.

### 6.3.5 Ultrasonic studies of multiple ground state configurations

The models represented by Fig. 6.11 and by Fig. 6.14 have one common feature, namely, that the tetrahedral molecular ion has two rotationally equivalent configurations at the substitutional lattice site which are separated by a large energy barrier due to steric effects and which, in fact, have slightly different energies due to local strain gradients in the crystal. For the first model, IR active librational sidebands should occur at frequencies near the vibrational mode value while for the second model low lying librational states are not required.

A measurement of the temperature-dependent absorption of 10 MHz ultrasound in RbBr, KI and RbI crystals doped with  $\text{ReO}_4^-$  has produced the first direct experimental identification of a two-configuration energy barrier associated with this defect-lattice system[6.54]. The loss peak which is shown in Figure 6.15 stems from an activation process with a barrier height of 60 meV for RbBr, 50 meV for KI and 30 meV for RbI. The decreasing barrier height with increasing lattice constant may account for the observation that spectral holes are burned and erased most easily in the RbI host.

The combination of ultrasound with the persistent spectroscopic effects has led to the development of a new phase-insensitive optical detector for ultrasonic waves in solids[6.55]. When ultrasonic waves are applied to an alkali halide which contains persistent holes or pegs the hole depth or peg height is modulated. This effect occurs because the local ultrasonic strain introduces a variety of frequency shifts which add up to a broadening of the persistent feature. Since, at the hole's (peg's) center frequency, the absorption can only increase (decrease) due to these frequency shifts; the transmitted signal reflects the rectified displacement. Such a process is completely independent of the phase of the ultrasound, provided that the acoustic wavelength is smaller than the beam diameter.

An estimate of the sensitivity of this new optical method of ultrasonic detection has shown that for the  $\text{ReO}_4^-$  molecule an ultrasonic wave amplitude of  $1 \text{ \AA}$  should be easily detectable. Even more sensitivity can be obtained by using the persistent photochemical hole of the  $\text{F}_3^+$  center in NaF where it was predicted that for 10 MHz sound an amplitude of  $10^{-2} \text{ \AA}$  could be detected [6.55]. A recent study of this defect-lattice system [6.56] has confirmed and extended these ideas to the problem of hole detection. Phase-sensitive modulation of spectral holes at MHz frequencies has also been observed [6.57].

### 6.3.6 Conclusions on the $\text{ReO}_4^-$ system

The view that the vibrational modes of matrix-isolated molecules should have long relaxation times in the  $10\ \mu\text{m}$  wavelength region is not generally valid because other relaxation processes dominate multiphonon decay. The intrinsic symmetry and simplicity of the matrix-isolated  $\text{ReO}_4^-$  molecule in alkali halide crystals has enabled the determination of many aspects of the anharmonic decay process. At low temperatures the decay channel consists of multistep emission of other internal modes, localized modes and band phonons.

The burning, at extremely low laser powers, of persistent spectral holes and antiholes in inhomogeneously broadened vibrational modes in crystals indicates that tunable diode lasers can be used to measure the homogeneous width of vibrational modes of matrix-isolated molecules throughout the IR. From this work it appears that the burning of such holes and antiholes at low laser intensity is a general solid state phenomenon which can occur whenever the complete ground state of the system to be excited has configurational degeneracy.

Early models for persistent nonphotochemical hole burning have relied on configurational change during deexcitation to move centers from one configuration to another. The dynamics of persistent nonphotochemical spectral hole and peg formation in the  $\nu_3$  vibrational mode absorption of  $\text{ReO}_4^-$  molecules in alkali halide crystals can be understood qualitatively with a simple energy level picture in which nearly forbidden interconfiguration transitions are important. Whether or not such forbidden transitions also play a central role in explaining the earlier results on NPHB for electronic transitions in organic glasses remains to be seen.

## 6.4 Persistent Spectral Hole-Burning for $\text{CN}^-$ Molecules in Alkali Halide Crystals

### 6.4.1 Background information on matrix-isolated $\text{CN}^-$

The IR spectrum of  $\text{CN}^-$  matrix-isolated in alkali halide crystals has attracted interest for many years because of its intrinsic simplicity. Depending on the particular matrix, the room temperature vibrational spectrum takes on one of two characteristic shapes: for KCl, KBr, KI and RbCl the band shows a predominant double hump structure with a total width of  $\approx 50 \text{ cm}^{-1}$  (FWHM) while for NaCl and NaBr a single band is observed with a width of  $\approx 20 \text{ cm}^{-1}$  (FWHM) [6.58]- [6.61]. The temperature-dependent properties of the double hump are identical to those observed at low resolution for the stretch region of a polar diatomic in the gas phase; thus the spectra have been identified with the P and R branches of freely rotating  $\text{CN}^-$  in the solid. The absence of any room temperature P and R structure at the stretch frequency for the Na salt hosts indicates that the molecule is not free to rotate in these lattices.

A temperature dependent absorption spectrum [6.58] of the first overtone band of KBr:  $\text{CN}^-$  which illustrates this high temperature free-rotor-like behavior is presented in Fig. 6.16. The separation between the two maxima varies as  $T^{1/2}$  between 60 K and 300 K giving a rotational constant  $B \approx 1.2 \text{ cm}^{-1}$  which is quite a bit smaller than the undistorted  $\text{CN}^-$  free rotor value,  $B = 1.94 \text{ cm}^{-1}$  [6.36]. At temperatures below 60 K the spatial anisotropy produced by the local crystalline electric field becomes observable. The interpretation of the lowest temperature spectrum (ignoring tunneling for the moment) is as follows: the strong transition is a zero libron transition, the weak high frequency satellite, a one libron sum band and the faint low frequency satellite, a one libron difference band [6.35]. Within the zero libron band of width  $\approx 2.5 \text{ cm}^{-1}$  a tunnel splitting of  $\approx 1 \text{ cm}^{-1}$  was predicted but not observed

[6.58] when measurements were attempted with a spectral resolution of  $0.6 \text{ cm}^{-1}$ . Later stress dependent studies [6.62], [6.63] demonstrated that the equilibrium orientations of the molecule in the potassium halide salts are directed along the equivalent  $\{111\}$  axes of the face centered cubic lattice site.

In the most recent spectroscopic investigation with a grating instrument which was carried out at a spectral resolution of  $0.1 \text{ cm}^{-1}$ , the tunneling structure for  $\text{CN}^-$  in KCl, KBr and KI hosts has been resolved [6.63]. A doublet split by  $2.5 \text{ cm}^{-1}$  in KCl is interpreted as the Stokes and anti-Stokes components of combined vibration-tunneling transitions [6.63]. With increasing lattice constant of the host ( $\text{KCl} \rightarrow \text{KI}$ ) the band shape shifts from two satellite peaks to a central line. The relative strengths of the central line compared to the two satellites vary from sample to sample for a given host depending on growth procedures; hence, it is concluded that the satellites identify those molecules which can tunnel and the central line, those which can not. Apparently, some  $\text{CN}^-$  molecules are always pinned in the lattice because of interactions with nearby impurities, internal strains, or other crystal defects [6.63].

#### 6.4.2 High resolution FTIR spectroscopy in the $\text{CN}^-$ stretch region

Figure 6.17a shows the low temperature absorption coefficient in the stretch mode frequency region at a resolution of  $0.04 \text{ cm}^{-1}$  for a KBr crystal doped with 0.05 mole % KCN [6.12], [6.13]. The vertical dashed line in the figure divides the spectrum into two frequency intervals. The absorption lines which occur at frequencies larger than  $2100 \text{ cm}^{-1}$  are associated with different isotopes of the linear molecule  $\text{NCO}^-$ , a common impurity in the KCN dopant. The linewidths of these transitions are all about  $0.05 \text{ cm}^{-1}$  (FWHM) and the frequencies are given in Table 6.2. None of these features show spectral hole burning.

The absorption lines at frequencies below  $2100\text{ cm}^{-1}$  in Fig. 6.17a are all associated with the  $\text{CN}^-$  stretch vibration in some way or other and the complexity of this spectrum is quite surprising [6.13]. Again the center frequencies, line identifications and hole burning results are summarized in Table 6.2. The fine structure near the main ( $^{12}\text{C}^{14}\text{N}^-$ ) absorption line can be seen more clearly in Fig. 6.17b where the spectrum of a lower concentration sample (0.01 mole % KCN) is displayed. This spectrum is characterized by one strong central line with a large linewidth ( $\approx 0.2\text{ cm}^{-1}$  FWHM) surrounded by lines which have much narrower linewidths ( $\approx 0.04\text{ cm}^{-1}$  FWHM). In the figure these satellite lines are labeled  $\alpha_1$ ,  $\alpha_2$ ,  $\gamma_1$ ,  $\gamma_2$ ,  $\gamma_3$  and  $\gamma_4$ .

The spectral shapes in Fig. 6.17b are somewhat different from those reported by *Beyeler* [6.63] for the same impurity concentration. His three components of equal strength ( frequency positions labeled by the arrows in the figure ) are to be compared with the single strong and weak satellite transitions shown here. The hole burning measurements reported by *Spitzer et al.* [6.12], [6.13] indicate that both the central line and related broad structure should be attributed to tunneling  $\text{CN}^-$  and the ultrasharp lines, to  $\text{CN}^-$  molecules frozen in direction by other nearby impurities in the crystal. With a broad band source an FTIR resolution of  $\approx 0.04\text{ cm}^{-1}$  is required to spectrally resolve these two types of centers in the region of overlap.

#### 6.4.3 Hole burning in the $\text{CN}^-$ stretch mode region

No hole burning has been detected in the main line shown in Fig. 6.17b but the sharp lines labeled  $\alpha_1$ ,  $\alpha_2$ ,  $\gamma_1$ ,  $\gamma_2$ ,  $\gamma_3$  and  $\gamma_4$  all show PIRSH's when probed with a diode laser [6.12], [6.13]. The signatures are very different from that found for the spherical top molecule  $\text{ReO}_4^-$ . Here, for each absorption line, the oscillator strength removed from the laser frequency does not reappear at another frequency within the inhomogeneously broadened line.

Examples of hole burning in the three absorption lines  $\alpha_1$ ,  $\alpha_2$ , and  $\gamma_1$  are shown in Fig. 6.18. Figure 6.18a shows a hole burned in the  $\alpha_1$  line which can be made 100 % deep but which washes out after about three minutes. The lines  $\gamma_2$ ,  $\gamma_3$  and  $\gamma_4$  (not shown) display a similar erasing behavior. Only a shallow hole can be burned in the  $\alpha_2$  line (shown in Fig. 6.18b) which erases in about 30 sec. Figure 6.18c shows the  $\gamma_1$  mode before and after two holes have been burned in it. These holes which can be made 100 % deep have the interesting property that they are permanent as long as the sample is maintained at liquid helium temperatures.

The temperature stability of the holes burned in the  $\gamma_1$  band has been determined by sweeping the spectrum with a low intensity probe beam while the sample temperature is varied [6.13]. Scans at four different temperatures are shown in Fig. 6.19: trace (a) of a sample at 1.7 K displays a spectrum which contains two holes, trace (b), the same sample at 15 K, trace (c), at 25 K and trace (d), at 35 K. At this highest temperature the spectrum appears nearly featureless yet upon recooling to 1.7 K the original spectral shape is recovered. Erasing does not become noticeable until the sample temperature is cycled up to about 48 K.

A systematic study of crystals double doped with  $\text{CN}^-$  and with different cation and anion dopants demonstrates that the vibrational center which produces the  $\gamma_1$  band is a  $\text{CN}^-$  molecule with a near neighbor  $\text{Na}^+$  impurity replacing one of the  $\text{K}^+$  host ions [6.63].

#### 6.4.4 A study of the $\text{CN}^-:\text{Na}^+$ center dynamics

##### 6.4.4.1 Fluorescence

Solid state vibrational fluorescence was first observed in 1972 for CO matrix-isolated in van der Waals solids [6.18] and somewhat later for isomorphic  $\text{CN}^-$  in ionic crystals [6.64]-

[6.67] . Subsequent direct vibrational excitation studies of the fluorescence from matrix-isolated  $\text{CN}^-$  at low temperatures have shown the importance of an efficient vibrational energy exchange process when the concentration exceeds  $\approx 0.05$  mole % which ultimately led to the first solid state vibrational laser [6.67]- [6.70] . This same vibrational energy exchange process has been used to determine the excited state vibrational lifetime of the  $\text{CN}^- : \text{Na}^+$  center [6.13].

For low  $\text{CN}^-$  concentration at 1.7 K the time-resolved fluorescence signal from the  $1 \rightarrow 0$  transition gives an excited state decay time of 27 msec; however, when the fundamental vibration of a high concentration sample is pumped the fluorescence signature is completely different. Figure 6.20 shows the emission spectrum for  $\text{KBr} + 0.12$  mole %  $\text{KCN} + 0.2$  mole %  $\text{NaBr}$  at 1.7 K. At this high  $\text{CN}^-$  concentration a series of sharp emission lines appear at frequencies below the pump frequency. These emission features result from the electric-dipole mediated V-V transfer process between  $\text{CN}^-$  molecules. This V-V transfer not only leads to population of highly excited vibrational states and isotope-shifted states of the  $\text{CN}^-$  molecule but also to a large population in the first excited state of the  $\text{CN}^- : \text{Na}^+$  center. To conserve energy in the transfer from a singly excited  $\text{CN}^-$  donor to the  $\text{CN}^- : \text{Na}^+$  acceptor a lattice phonon is emitted at a frequency equal to the energy difference. Since this energy deficit is much larger than the thermal energy  $kT$  the back reaction is not allowed and the vibrational energy is funneled from the laser pumped  $\text{CN}^-$  molecules into the  $\gamma_1$  centers.

Measurement of the time resolved fluorescence signal from the  $\gamma_1$  center and from the isolated  $^{13}\text{C}^{14}\text{N}^-$  center give lifetimes of 10 msec and 25 msec, respectively. The shorter lifetime for the  $\gamma_1$  center could stem from its higher concentration so the best estimate of its excited state lifetime,  $T_1$ , is between 10 msec and 25 msec; hence, the vibrational mode lifetime of the  $\text{CN}^-$  molecule is not radically changed by the presence of an impurity ion [6.13].



#### 6.4.4.2 Hole burning and $\gamma_1$ center geometry

##### 6.4.4.2.1 Polarization studies

Polarized spectral hole burning spectroscopy has established the crystallographic orientation of the  $\gamma_1$  center in the lattice. The main results are summarized in Fig. 6.21. The top two traces for the probe beam show the  $\gamma_1$  line before and after hole burning with the laser beam propagating along a [001] axis and the probe and burn polarizations parallel to the [100] crystal axis. When the probe polarization is rotated by  $90^\circ$  to be perpendicular to the burn polarization as is shown in the bottom two traces then no absorption change is observed. From these experimental results it is clear that the  $\gamma_1$  center cannot be oriented along the  $\langle 111 \rangle$  crystal axes which are the equilibrium directions for the molecule in the unperturbed lattice. The polarization results are consistent with the molecule being directed along one of the six  $\langle 100 \rangle$  axes with the particular axis determined by the location of the near neighbor  $\text{Na}^+$  impurity [6.13].

##### 6.4.4.2.2 Union of broadband and hole burning techniques

The frequency shift of the hole-burned product state to a region outside of the  $\gamma_1$  inhomogeneous line makes it difficult to locate directly because of the small continuous tuning range of a diode laser. The solution of this problem has been to use another unusual property of the  $\gamma_1$  mode hole burning which is shown in Fig. 6.22. Figure 6.22a demonstrates that by sweeping the diode laser frequency over a fixed interval for about 2 min at an intensity of  $500 \text{ mW/cm}^2$  a slot can be milled in the absorption line. If the sweeping interval is increased to include the entire absorption line then the inhomogeneous line is erased ( Fig. 6.22b) after 80 min

To locate the vibrational absorption of the product state the diode laser is used as the pump in conjunction with a FTIR interferometer which provides a broad band probe beam [6.13]. Since the FTIR resolution is only  $0.04 \text{ cm}^{-1}$  the diode is swept over the  $0.04 \text{ cm}^{-1}$  wide  $\gamma_1$  line to burn away the most of the absorption for one polarization. After erasing the  $\gamma_1$  mode an FTIR spectrum is obtained, then the sample is warmed to 50 K to recover the  $\gamma_1$  mode, cooled back down to 1.7 K, and another spectrum obtained. The spectra are presented in Fig. 6.23: the top trace displays the FTIR absorption spectrum before erasing and the bottom trace shows the difference in absorption coefficients [ $\gamma_1$  (erased) -  $\gamma_1$  (burned)]. Erasing the  $\gamma_1$  mode produces the  $\gamma_1'$  mode at a higher frequency which is nearly coincident with that of the unperturbed  $\text{CN}^-$  molecule; in addition, the polarization of the  $\gamma_1$  and  $\gamma_1'$  modes is the same as are the integrated absorption strengths. Note that none of the other sharp  $\text{CN}^-$  complex lines have changed so the particular geometrical arrangement for  $\text{CN}^-: \text{Na}^+$  which produces the  $\gamma_1$  mode is not the same as those which produce  $\gamma_2$ ,  $\gamma_3$  and  $\gamma_4$  absorption lines. These latter spectral lines must be caused by centers with distinctly different locations of the  $\text{Na}^+$  relative to the  $\text{CN}^-$ .

With the frequency position of the  $\gamma_1'$  mode identified it is now possible once again to use high resolution diode laser hole burning to explore its properties [6.13]. After the  $\gamma_1'$  mode has been populated a persistent spectral hole (FWHM  $\approx 100 \text{ MHz}$ ) can be burned in it. It is also possible to sweep the diode frequency and burn away the entire absorption line with the oscillator strength returning to the  $\gamma_1$  mode. Another interesting property is that the entire  $\gamma_1'$  mode can be erased by tuning the diode anywhere in the main  $\text{CN}^-$  stretch region. This nonresonant erasing is a consequence of the efficient V-V transfer process which can not only transfer an excitation in the crystal but also at the appropriate place transfer from an isolated  $\text{CN}^-$  to the higher frequency  $\gamma_1'$  center because the energy deficit is less than  $kT$ .

#### 6.4.4.4 Two-configuration model for hole production

The simplest hole burning model consistent with the polarization and photoproduct data is that the  $\text{CN}^-$  molecule rotates by  $180^\circ$  between the two states [6.13]. Since the  $\text{CN}^-$  has a large elastic dipole moment it will preferentially align in the lattice to minimize the elastic energy. The  $\text{CN}^-$  molecular axis points at the nearest neighbor  $\text{Na}^+$ , and the four nearest neighbor  $\text{K}^+$  ions in the plane perpendicular to the molecular axis relax inward to produce the large barrier to rotation. The two states correspond to the two equivalent directions for the elastic dipole axis with the inequivalence produced by the interaction of the  $\text{CN}^-$  electric dipole and the  $\text{Na}^+$  impurity.

In the two configuration model, which is drawn to scale in Fig. 6.24, only one state is populated at low temperature because the energy separation between the two configurations,  $\epsilon = 150$  K. If, at low temperature, some fraction of centers are put in the high energy state they remain there because of the large energy barrier,  $V = 1500$  K, which prohibits classical reorientation and makes reorientation by tunneling extremely unlikely. At high temperatures thermal activation over the barrier becomes possible, thermal equilibrium is restored and the relative population in the two configurations is governed by the Boltzmann factor.

The energy mismatch between the ground state energies in the two configurations has been obtained from high resolution broad band measurements of the absorption profile at elevated temperatures [6.13]. By 50 K all of the sharp lines near the stretch mode have melted into the characteristic P and R bands associated with free rotor behavior of the isolated  $\text{CN}^-$ ; however, the  $\gamma_1$  mode and the  $\text{NCO}^-$  modes remain distinct and narrow in width: the former because it is pinned by the  $\text{Na}^+$  impurity and the latter because the long linear molecule is pinned by the lattice. The fact that  $\text{NCO}^-$  does not fluoresce while both the broad and sharp modes of  $\text{CN}^-$

do clearly demonstrates that the vibrational mode lifetime cannot readily be estimated from the measured widths of spectral lines.

The  $\gamma_1'$  mode becomes observable in normal FTIR spectroscopy at about 50 K which is the same temperature at which holes in the  $\gamma_1$  mode erase rapidly. Hole refilling data at elevated temperatures together with the classical Arrhenius relaxation approximation provide a convenient way for determining the barrier height shown in Fig. 6.24.

#### 6.4.5 Other $\text{CN}^-$ complexes

The interesting behavior obtained for the  $\text{CN}^- : \text{Na}^+$  center has not been duplicated when other cations are added to the host [6.13]. Figure 6.25 shows the influence of different alkali impurity ions on the  $\text{CN}^-$  stretch mode region. Since the same concentration of alkali dopant has been used in each case, the spectral features can be compared directly with the  $\text{Na}^+$  case which is shown in Fig. 6.25a. Figure 6.25b indicates that the perturbations produced by double doping with LiBr cause six new lines to appear. Sharp lines are observed at all temperatures and the line positions for 1.7 K are tabulated in Table 6.2. The  $\gamma$  lines involve  $\text{CN}^- : \text{Li}^+$  and the  $\beta$  lines,  $\text{CN}^- : \text{Li}^+$  (pairs). Double doping with RbBr produces a single new line close to the main  $\text{CN}^-$  stretch mode frequency (Fig. 6.25c) which disappears by a temperature of 25 K.

None of the sharp spectral lines induced by  $\text{Li}^+$  or  $\text{Rb}^+$  show persistent spectral effects. This null result is surprising because both an alkali and a halide ( $\text{Cl}^-$ ) impurity ion have already been used successfully to obtain persistence and the two-configuration model illustrated in Fig. 6.24 should apply to all of these isoelectronic dopant cases. The fact that  $\text{CN}^-$  ion in conjunction with monovalent ions in KBr may or may not give rise to persistent

effects in the vibrational spectrum suggests that the physical process behind the hole burning is not yet clearly identified.

## 6.5 Conclusion

### 6.5.1 Comparison of the three types of vibrational hole-burning systems

The low power diode laser source, which in principle can be fabricated and tuned to cover any region of the vibrational infrared, is an effective hole-burning probe for the  $\nu_{17}$  mode of the *trans* conformation of  $\text{CH}_2\text{F}-\text{CH}_2\text{F}$  matrix-isolated in Ar, Kr or  $\text{N}_2$ . From the temperature dependence of the spectral holes together with some assumptions about the dephasing mechanism, an estimate of the vibrational excited state lifetime has been made while from polarization studies molecular tunneling or free rotation of the molecule in the host can be ruled out. Fixed frequency  $\text{CO}_2$  laser measurements have provided valuable additional information on the hole burning properties of this molecule in Xe as well as the hosts listed above. At a laser intensity which is about  $10^4$  times larger than obtained from the diode but still small compared to the values required to produce nonlinear effects, vibrational photochemical hole burning in the form of *trans* - *gauche* conversion is observed for the Kr and Xe hosts but not for Ar. Finally, IR photophysical hole-burning has been found for three different molecular aggregates in Ar and  $\text{N}_2$  matrices.

The holes and antiholes burned in the  $\text{ReO}_4^- \nu_3$  vibrational mode have a variety of novel properties, some similar to the PIRSH's detailed in Sec. 6.2. Because both  $T_1$  and  $T_2$  have been determined for this vibrational mode from transient techniques, it has been possible to demonstrate, at least in this defect-lattice system, that the transient and persistent hole burning spectral widths are the same. The persistent properties of this combination appear to involve reorientation of the impurity during IR excitation to the excited vibrational state. A photon-induced reorientation model accounts for most of the observed properties. This study demonstrates that persistence is possible even for a spherical top molecule located in a cubic

site. Ultrasonic measurements have shown that because of steric effects the two rotationally equivalent configurations for this tetrahedral molecule in a substitutional lattice site are separated by a large energy barrier and made inequivalent by the local strain gradient at the molecular site.

A different kind of PIRSH production has been observed for  $\text{CN}^-$  complexes in KBr crystals. These complexes consist of the  $\text{CN}^-$  molecule together with an alkali or halogen ion impurity at a nearby lattice site. Of the fourteen new centers identified, six of them show persistent hole burning when the perturbed  $\text{CN}^-$  stretch mode is probed with a low power diode laser. One extremely stable defect complex:  $\text{CN}^- : \text{Na}^+$ , which both fluoresces and hole burns, has been investigated in some detail. By combining broadband Fourier transform interferometry with narrow band diode laser hole burning it has been demonstrated that this particular persistent effect occurs when, during vibrational de-excitation, the  $\text{CN}^-$  molecule flips by  $180^\circ$  between inequivalent energy configurations generated by the presence of the nearby  $\text{Na}^+$  ion. For this system the measured hole width has no connection to the excited state lifetime,  $T_1$ , which is determined from a fluorescence measurement. This result is completely different from that found for the more complex  $\text{ReO}_4^-$  and DFE molecules and demonstrates that, in general, the hole width cannot be used to find the excited vibrational state lifetime. Although the persistent effect can no longer by itself be used to extract information about the decay process, it still provides a high resolution probe of the center and its environment as this study demonstrates.

## 6.5.2 Systems which do not show PIRSH's

### 6.5.2.1 Derivatives of the $\text{CN}^-$ molecule

The identification of the essential components for persistent IR spectral hole burning in solids requires cataloging those systems which do not produce PIRSH as well as those which do. Inspection of Table 6.2 shows that, for the 21 molecular centers in alkali halide crystals in which diode laser hole burning has been attempted, PIRSH's have not been found in two thirds of these cases. The absence of hole burning for  $\text{NCO}^-$  can be rationalized on the grounds that the linear triatomic molecule is too long to fit easily into a substitutional lattice site and these large steric effects from the lattice inhibit the reorientation of the molecule between equivalent sites when it is excited by a vibrational quantum.

The isolated  $\text{CN}^-$  molecule represents the opposite limit. The molecule is small enough to tunnel rapidly among the equivalent  $\{111\}$  orientations so that the thermal ground state is composed from a symmetric combination of this configuration set so that PIRSHs would not be expected to form unless another configuration set, say  $\{100\}$  orientations, was separated by a large energy barrier but nearby in ground state energy. The experimental results show that this is not the case for the KBr host.

Both the  $\text{Na}^+$  and  $\text{Cl}^-$  ions are effective in lifting this tunneling degeneracy for the  $\text{CN}^-$  molecule so that PIRSH's can occur while, on the other hand, PIRSH's are not found for crystals similarly doped with  $\text{Li}^+$  or  $\text{Rb}^+$ . Given the simple geometric model described in Sec. 6.4, in which the  $\text{CN}^-$  molecule during vibrational de-excitation simply rotates by  $180^\circ$  with respect to the monatomic impurity site, this null result is quite surprising. Presumably, a transition from the excited vibrational and ground rotational state to a ground vibrational but excited rotational state in the first configuration puts the system in a region of low barrier height so that it can reach the second configuration. The picture should be the same whatever the monatomic impurity. The fact that  $\text{CN}^-$  ions in conjunction with monovalent impurity



ions in KBr may or may not give rise to PIRSH's indicates that the physical process behind the cross relaxation effect is not yet clearly defined.

Null results also have been obtained for another group of  $\text{CN}^-$  complexes in KCl [6.71]. When  $\text{O}_2^-$  is diffused into a previously  $\text{CN}^-$  doped KCl or KBr crystal the absorption lines above  $2100 \text{ cm}^{-1}$  increase in strength indicating that some  $\text{CN}^-$  is converted to  $\text{NCO}^-$ ; in addition, a large number of new lines appear below  $2100 \text{ cm}^{-1}$  in the  $\text{CN}^-$  stretch region indicating that  $\text{CN}^- : \text{O}_2^-$  complexes have formed. The absorption spectra for the KCl host are shown in Fig. 6.26. The KCl:  $\text{CN}^-$  low temperature spectrum (before heating the sample in  $\text{O}_2$  gas) is shown in Fig. 6.26a. The same crystal after heat treatment is shown in Fig. 6.26b. All of the new absorption lines which must stem from a variety of defect geometries have spectral widths (FWHM) of about  $0.05 \text{ cm}^{-1}$ . Although these absorption lines appear in the same frequency region as the  $\gamma$  absorption lines described in Sec. 6.4, PIRSHs have not been found for any of these new centers. Since the statics and dynamics of these centers are unknown the only conclusion which can be drawn from these measurements together with Table 6.2 is that most  $\text{CN}^-$  complexes do not hole burn.

#### 6.5.2.2 Spherical top molecules which contain hydrogen

The systematic investigation of the transient and persistent hole burning properties of the  $\nu_3$  mode for  $\text{ReO}_4^-$  molecules in alkali halide crystals has produced a detailed understanding of the microscopic mechanisms responsible for the decay of the excited vibrational state and for the appearance of PIRSH's. The key component for the decay process is that the  $\nu_3$  mode can decay into the low lying  $\nu_4$  mode of this spherical top molecule which is near in energy to the phonon spectrum so that a low order multi-phonon process is probable.

A recent study [6.72], [6.73] has focused on the vibrational relaxation of a different spherical top molecule,  $\text{BH}_4^-$ , so that the lowest frequency  $\nu_4$  mode occurs in the  $\text{CO}_2$  laser wavelength region. Since, at liquid helium temperature, the  $\nu_4$  mode frequency is slightly above than the 9R branch of the  $\text{CO}_2$  laser and the  $\text{BD}_4^-$  mode is slightly below the 10P branch, both  $\text{BH}_4^-$  and  $\text{BD}_4^-$  molecules are diffused into the alkali halide at the same time. Because of isotope exchange, molecules of  $\text{BH}_3\text{D}^-$ ,  $\text{BH}_2\text{D}_2^-$ , and  $\text{BHD}_3^-$  also appear in the crystal and the lower frequency modes of these molecules are in the  $\text{CO}_2$  laser tuning range.

Of interest here is the  $\nu_{4b}$  vibrational mode of  $\text{BH}_2\text{D}_2^-$  in KBr at low temperatures which is coincident with the strong  $\text{CO}_2$  laser line, 10P22 ( $942\text{ cm}^{-1}$ ). A comparison of the vibrational energy level diagrams for  $\text{ReO}_4^-$  and  $\text{BH}_2\text{D}_2^-$  is shown in Fig. 6.27. The lower case letters in the figure identify the three non-degenerate  $\nu_4$  modes of  $\text{BH}_2\text{D}_2^-$ , while both the  $\nu_3$  and  $\nu_4$  of  $\text{ReO}_4^-$  are threefold degenerate. The arrow indicates the transition pumped in each system by the  $\text{CO}_2$  laser. At low laser intensities no PIRSH is found for the  $\text{BH}_2\text{D}_2^- \nu_{4b}$  mode; furthermore, at high laser intensities of  $1\text{ MW/cm}^2$  no bleaching of the absorption band is observed. These null results are to be contrasted with the positive results obtained for the  $\text{ReO}_4^- \nu_3$  mode which already have been described in Sec. 6.3.

We now consider some of the reasons which may cause this optically inert behavior. Because of the small moment of inertia for  $\text{BH}_2\text{D}_2^-$ , free rotation or rapid tunneling among equivalent molecular orientations could eliminate the PIRSH possibility; however, the absence of transient bleaching is not so easy to explain. The nonradiative vibrational relaxation time of both HCl and DCl matrix-isolated in Ar [6.21], which is consistent with a relaxation process in which the rate determining step is vibration-rotation transfer, is relatively long ( $\approx 100\text{ }\mu\text{sec}$ ) when compared to the time for  $\text{BH}_2\text{D}_2^-$  estimated from the high intensity  $\text{CO}_2$  laser

measurement ( $< 20$  psec) yet in both cases the ratio of the mode frequency to the rotational constant is about the same.

Another difference between  $\text{ReO}_4^-$  and  $\text{BH}_2\text{D}_2^-$  is that the former has a very large mass (250 amu) and the latter very small (15 amu) when compared to the lattice ion mass. Although the  $\nu_{4b}$  mode is far removed from the normal phonon energies the small mass defect would be expected to produce a local mode with frequency above the normal band mode region. If the  $\nu_{4b}$  mode decay made use of this high frequency external mode then the decay would occur in lower order, hence be faster. Such a local mode has been observed for  $\text{BH}_4^-$  in RbI [6.74]. If this feature represents the important decay channel then four local modes plus one band mode are required to relax the excited vibrational state. This is the same order of multi-phonon decay that is required to explain the  $\text{ReO}_4^-$  data in Sec. 6.3 so the two relaxation times should be comparable. The experimental results show that the  $\nu_{4b}$  mode must relax at least three orders of magnitude faster than does the  $\text{ReO}_4^-$  vibration.

An important difference between the two systems is that a Fermi resonance exists between  $2\nu_4$  and  $\nu_3$  for the  $\text{BH}_2\text{D}_2^-$  molecule [6.74] but not for the  $\text{ReO}_4^-$  system. Because of the strong coupling between these two vibrational ladders the high laser intensity may simply populate both ladders so that saturation would be much harder to attain; however, a search in the infrared and visible has shown that no vibrational fluorescence occurs for this defect. In order to account for these data both a Fermi resonance and either a free-rotor-like degree of freedom or a local lattice mode are required to account for the rapid decay. The local mode or rotor states insure that the decay process is as fast as  $\text{ReO}_4^-$  ( $\approx 5$  nsec) and the Fermi resonance insures that a large reservoir of levels is available to suppress bleaching. Since the vibrational fluorescence radiative lifetime is  $\approx 1$  msec, this process is completely quenched by the much faster nonradiative decay channels.

### 6.5.3 Future prospects

#### 6.5.3.1 $\text{NO}_2^-$ in alkali halides

The nitrite molecule has a bent O-N-O structure with  $C_{2v}$  symmetry and optical and infrared measurements [6.75]- [6.80] have determined that when it is doped into the alkali halide crystal the symmetry axis of the  $\text{NO}_2^-$  molecule lies in a  $\langle 110 \rangle$  direction with the molecular plane in a (100) plane. The vibrational modes of this asymmetric top are:  $\nu_1$  (the high frequency symmetric stretch),  $\nu_2$  (the low frequency bending mode), and  $\nu_3$  (the intermediate frequency asymmetric stretch). For KCl, KBr and RbCl hosts molecular energy levels which correspond to free rotation, libration, and tunneling have been identified [6.75]- [6.79]. The KI results are very different probably because the molecule occupies an off-center position in the lattice so that both translation and rotation are strongly coupled together. It has been proposed that KI:  $\text{NO}_2^-$  may represent the most general case for motion of molecules in solid solution [6.77].

A preliminary report has appeared which describes PIRSH production in KBr:  $\text{NO}_2^-$  [6.81]. Probing the vibrational modes with tunable diode lasers reveals that PIRSH's occur in two of the three modes. The results are that : a) the  $\nu_1$  mode does not burn, b) the  $\nu_3$  mode burns with a hole width  $\approx 100$  MHz, and c) both the zero libron line and the sidebands of  $\nu_2$  burn with hole widths of 350 MHz and 1GHz, respectively. Additional experiments have shown that PIRSH's appear in the same modes for KCl and KI hosts as well. In all cases the missing oscillator strength relocates to a different polarization inside the inhomogeneous linewidth, unlike either the spherical top,  $\text{ReO}_4^-$ , or the  $\text{CN}^- : \text{Na}^+$  center. Similar studies may be possible on the isomorphic defect,  $\text{PO}_2^-$ .

The observation of PIRSH's in the internal modes of  $\text{KI: NO}_2^-$  opens up the possibility of generating holes in the external vibrational mode spectrum produced by the defect. Impurity induced spectral features, which occur in the gap of the lattice vibration frequencies for KI, have been attributed to translational modes of the  $\text{NO}_2^-$  ion in its cavity, high frequency librational modes, or perturbed lattice modes of the host crystal [6.37]. By pumping one of the internal modes of the molecule with a diode laser the molecule can be transferred from one elastically polarized configuration to another. Since this new configuration will have its own polarized external mode spectrum it may be possible to produce persistent holes in the far infrared by burning in the IR. Generation of such far IR spectra would provide the information required to properly interpret the present gap mode results and also to determine if external modes are inhomogeneously broadened.

#### 6.5.3.2 Disordered solids

The burning of PIRSH's in the modes of molecular impurities in alkali halides indicates that similar effects should be observable with some molecules embedded in any crystal lattice. In a more general sense one need not rely only on the molecule to produce more than one ground state configuration to support PIRSH dynamics since it is the total system -defect plus lattice- which is important. For example, in glasses it is known that at low energies the dynamics is dominated by the two-level tunneling states [6.82]. If the vibration of an impurity molecule in a glass is excited with a diode laser and the two level states (TLS) of the host change during the IR transition once again a persistent hole could appear. Measurements on impurity electronic transitions in organic glasses have already demonstrated that visible energy photons cause such a process (See Chapter 5 and Ref. [6.3]).

Once it is realized that either reorientation of the impurity molecule and/or rearrangement of the host can give rise to persistent hole burning features in the vibrational spectrum then complex molecular solids which have a large number of low lying conformational states should be particularly susceptible to this high resolution technique. Organic polymers appear to satisfy all of the necessary conditions. If holes could be produced in these materials then one would have high resolution information about the vibrational dynamics at specific polymer sites, information which is currently buried in the inhomogeneously broadened spectrum.

## ACKNOWLEDGEMENTS

The authors acknowledge the fruitful collaboration over the years with W. P. Ambrose, A. R. Chraplyvy, T. R. Gosnell, H. Lengfellner, and R. Spitzer on some of the results reported in this chapter. The authors also thank H. H. Günthard for permission to reprint Figs. 6.2 - 6.5 and V. Narayanamurti for permission to reprint Fig. 6.16. This work has been supported in part by U.S. Army Research Office Grants DAAG-29-79-C-0170, DAAG-29-83-004, and DAAG-29-84-0034; by National Science Foundation Grants 79-24008 and DMR-80-08546; by National Science Foundation Grant No. DMR-76-81083 through the Cornell Materials Science Center; and by the U. S. Office of Naval Research.

## REFERENCES

- 6.1 J. M. Hayes, R. P. Stout, G. J. Small: J. Chem. Phys. 74, 4266 (1981).
- 6.2 F. G. Patterson, H. W. H. Lee, R. W. Olson, M. D. Fayer: Chem. Phys. Lett. 84, 59 (1981).
- 6.3 G. J. Small: "Persistent Nonphotochemical Hole Burning and the Dephasing of Impurity Electronic Transitions in Organic Glasses", in Spectroscopy and Excitation Dynamics of Condensed Molecular Systems, ed. by V. M. Agranovitch and R. M. Hochstrasser, (North-Holland, Amsterdam 1983), pp. 515-554.
- 6.4 J. T. Yardley: "Dynamic Properties of Electronically Excited Molecules" in Chemical and Biochemical Applications of Lasers, ed. by C. B. Moore (Academic Press, New York 1974), Vol. I, pp. 231-279.
- 6.5 See for example, M. Poliakoff, N. Breendon, B. Davies, A. McNeish, J. J. Turner: Chem. Phys. Lett. 56, 474 (1978).
- 6.6 M. Dubs, H. H. Günthard: Chem. Phys. Lett. 64, 105-107 (1979).
- 6.7 M. Dubs, H. H. Günthard: J. Mol. Structure 60, 311-316 (1980).
- 6.8 M. Dubs, L. Ermanni, H. H. Günthard: J. Mol. Spectr. 91, 458-491 (1982).



- 6.9 W. E. Moerner, A. J. Sievers, R. H. Silsbee, A. R. Chraplyvy, D. K. Lambert: Phys. Rev. Lett. 49, 398 (1982).
- 6.10 W. E. Moerner, A. R. Chraplyvy, A. J. Sievers, R. H. Silsbee: Phys. Rev. B 28, 7244 (1983); Phys. Rev. B 29, 4791 (1984).
- 6.11 T. R. Gosnell, A. J. Sievers, R. H. Silsbee: Phys. Rev. Lett. 52, 303 (1984).
- 6.12 R. C. Spitzer, W. P. Ambrose, A. J. Sievers: Opt. Lett. 11, 428-430 (1986).
- 6.13 R. C. Spitzer, W. P. Ambrose, A. J. Sievers: Phys. Rev. B (to be published, 1986).
- 6.14 See for example, Vibrational Spectroscopy of Trapped Species, ed. by H. E. Hallam (John Wiley & Sons, New York 1973).
- 6.15 B. M. Chadwick: "Matrix Isolation", in Molecular Spectroscopy, ed. by R. F. Barrow, D. A. Long, D. J. Millen (The Chemical Society, London 1975), p. 281cf.
- 6.16 See for example, Cryochemistry, ed. by M. Moskovits and G. A. Ozin (John Wiley and Sons, New York 1976).
- 6.17 B. I. Swanson, L. H. Jones: "High Resolution Infrared Studies of Site Structure and Dynamics for Matrix isolated Molecules" in Vibrational Spectra and Structure, A Series of Advances, ed. by J. R. Durig (Elsevier, Amsterdam 1983) Vol. 12, pp. 1-67.

- 6.18 H. Dubost, L. Abouaf-Marguin, F. Legay: Phys. Rev. Lett. 29, 145 (1972).
- 6.19 F. Legay: "Vibrational Relaxation in Matrices", in Chemical and Biochemical Applications of Lasers, ed. by C. B. Moore (Academic Press, New York 1977), Vol. II, pp. 43-86.
- 6.20 H. Dubost: Ber. Bunsenges. Phys. Chem. 82, 112 (1978).
- 6.21 J. M. Wiesenfeld C. B. Moore: J. Chem. Phys. 70, 930-946 (1979).
- 6.22 H. Dubost, R. Charneau: Chem. Phys. 41, 329 (1979).
- 6.23 H. Dubost, A. Lecuyer, R. Charneau: Chem. Phys. Lett. 66, 191 (1979).
- 6.24 L. Abouaf-Marguin, B. Gauthier-Roy: Chem. Phys. 51, 213 (1980).
- 6.25 B. Gauthier-Roy, L. Abouaf-Marguin, F. Legay: Chem. Phys. 46, 31 (1980).
- 6.26 L. Abouaf-Marguin, P. Boissel, B. Gauthier-Roy: J. Chem. Phys. 75, 495 (1981).
- 6.27 H. Dubost: "Spectroscopy of Vibrational and Rotational Levels of Diatomic Molecules in Rare Gas Crystals" in Inert Gases: Potentials, Dynamics, Energy Transfer in Doped Crystals, ed. by M. L. Klein (Springer Verlag, New York 1984), pp. 145-257.
- 6.28 M. Hartig, H. Dubost: J. Lumin. 24/25, 643 (1981).

- 6.29 M. Hartig, H. Dubost: Phys. Rev. Lett. 49, 715 (1982).
- 6.30 I. Maslakowez: Z. Physik 51, 696 (1928).
- 6.31 J. C. Decius, A. Maki: J. Chem. Phys. 28, 1003 (1958).
- 6.32 W. C. Price, W. F. Sherman, G. R. Wilkinson: Proc. Roy. Soc. A255, 5 (1960).
- 6.33 W. C. Price, W. F. Sherman, G. R. Wilkinson: Spectrochim. Acta 16, 663 (1960).
- 6.34 F. Lüty: J. de Physique, Coll. C4, 120 (1967).
- 6.35 V. Narayanamurti, R. O. Pohl: Rev. Mod. Phys. 42, 201 (1970).
- 6.36 W. F. Sherman, G. R. Wilkinson: "Infrared and Raman Studies on the Vibrational Spectra of Impurities in Ionic and Covalent Crystals", in Vibrational Spectroscopy of Trapped Species, ed. by H. E. Hallam (John Wiley and Sons, New York 1973), pp. 246-318.
- 6.37 A. S. Barker, A. J. Sievers: Rev. Mod. Phys. 47, Supp. 2, 1-179 (1975).
- 6.38 R. K. Ahrenkiel, J. F. Figueira, C. R. Phipps, D. J. Dunlavy, S. J. Thomas, A. J. Sievers: Appl. Phys. Lett. 33, 705-707 (1978).
- 6.39 T. Gethins: Can. J. Phys. 48, 580 (1970).

- 6.40 H. W. Moos: J. Lumin. 1-2, 106 (1970).
- 6.41 A. J. Sievers: Cryst. Latt. Def. and Amorph. Mat. 12, 441 (1985).
- 6.42 A. R. Chraplyvy, A. J. Sievers: Opt. Lett. 3, 112 (1978).
- 6.43 A. R. Chraplyvy, W. E. Moerner, A. J. Sievers: Opt. Lett. 6, 254 (1981).
- 6.44 A. R. Chraplyvy, W. E. Moerner, A. J. Sievers: Opt. Lett. 6, 431 (1981).
- 6.45 W. E. Moerner, A. J. Sievers, A. R. Chraplyvy: Phys. Rev. Lett. 47, 1082 (1981).
- 6.46 W. E. Moerner, A. R. Chraplyvy, A. J. Sievers: Phys. Rev. B 29, 6694 (1984).
- 6.47 P. Huber-Wälichli, H. H. Günthard: Chem. Phys. Lett. 30, 347-351 (1975).
- 6.48 M. Poliakoff, J. I. Turner: "Infrared Laser Photochemistry in Matrices", in Chemical and Biochemical Applications of Lasers, ed. by C. Bradley Moore, Vol. 5 (Academic Press, New York 1980), pp. 175-216.
- 6.49 H. Frei, L. Fredin, G. C. Pimentel: J. Chem. Phys. 74, 397-411 (1981); H. Frei, G. C. Pimentel: J. Chem. Phys. 78, 3698 (1983).
- 6.50 P. Felder, H. H. Günthard: Chem. Phys. Lett. 88, 473-476 (1982).

- 6.51 P. Felder, H. H. Günthard: Chem. Phys. 85, 1 (1984).
- 6.52 W. E. Moerner: Ph.D. Thesis, Cornell University, Ithaca, New York 1982  
(unpublished).
- 6.53 M. R. Mohammad, W. F. Sherman: J. Phys. C: Solid State 14, 283 (1981).
- 6.54 H. Lengfellner, A. J. Sievers: Phys. Rev. B31, 2591 (1985).
- 6.55 H. Lengfellner, T. R. Gosnell, R. Tkach, A. J. Sievers: Appl. Phys. Lett. 43, 437  
(1983).
- 6.56 A. L. Huston, W. E. Moerner: J. Opt. Soc. Amer. B1, 349 (1984).
- 6.57 W. E. Moerner, A. L. Huston: Appl. Phys. Lett. 48, 1181 (1986).
- 6.58 W. D. Seward, V. Narayanamurti: Phys. Rev. 148, 463 (1966).
- 6.59 G. R. Field, W. F. Sherman: J. Chem. Phys. 47, 2378 (1967).
- 6.60 M. A. Cundill, W. F. Sherman: Phys. Rev. 168, 1007 (1968).
- 6.61 R. Callender, P. Pershan: Phys. Rev. A2, 672 (1970).
- 6.62 F. Lüty: Phys. Rev. B10, 3677 (1974).

- 6.63 H. U. Beyeler: Phys. Rev. B11, 3078 (1975).
- 6.64 Y. Yang, F. Lüty: Phys. Rev. Lett. 51, 419 (1983).
- 6.65 K. P. Koch, Y. Yang, F. Lüty: Phys. Rev. B29, 5840 (1984).
- 6.66 T. R. Gosnell, R. W. Tkach, A. J. Sievers: Solid State Commun. 53, 419-421 (1985).
- 6.67 R. W. Tkach, T. R. Gosnell, A. J. Sievers: Opt. Lett. 9, 122 (1984).
- 6.68 T. R. Gosnell, R. W. Tkach, A. J. Sievers: J. Lumin. 31-32, 166 (1984).
- 6.69 T. R. Gosnell, R. W. Tkach, A. J. Sievers: Infrared Phys. 25, 35 (1985).
- 6.70 T. R. Gosnell, A. J. Sievers, C. R. Pollock: Opt. Lett. 10, 125 (1985).
- 6.71 R. C. Spitzer, Ph.D. Thesis, Cornell University, 1987 (unpublished).
- 6.72 D. M. Kammen, T. R. Gosnell, R. W. Tkach, A. J. Sievers: Bull. Amer. Phys. Soc. 29, 502 (1984).
- 6.73 D. M. Kammen, T. R. Gosnell, R. W. Tkach, A. J. Sievers: J. Chem. Phys. (to be published).
- 6.74 M. I. Memon, W. F. Sherman, G. R. Wilkinson: Spectrochim. Acta, A37, 461 (1981).

- 6.75 T. Timusk, W. Staude: Phys. Rev. Lett. 13, 373 (1964)
- 6.76 C. D. Lytle, A. J. Sievers: Phys. Rev. Lett. 14, 271-273 (1965).
- 6.77 V. Narayanamurti, W. D. Seward, R. O. Pohl: Phys. Rev. 148, 481-494 (1966).
- 6.78 R. Avarmaa, L. Rebane: Phys. Status Solidi 35, 107 (1969).
- 6.79 A. R. Evans, D. B. Fitchen: Phys. Rev. B2, 1074 (1970).
- 6.80 K. K. Rebane, L. A. Rebane: Pure and Appl. Chem. 37, 161-181 (1974).
- 6.81 W. P. Ambrose, A. J. Sievers: Bull. Amer. Phys. Soc. 31, 278 (1986).
- 6.82 See for example, Amorphous Solids, ed. by W. A. Phillips, Topics Curr. Phys., Vol. 24 (Springer, Berlin, Heidelberg 1981).

## FIGURE CAPTIONS

Figure 6.1. Schematic diagram showing the generalized mechanism producing persistent spectral hole burning in a vibrational mode.

Figure 6.2 Diode laser spectrum of the matrix-split  $\nu_{17}$  mode, *trans* conformation of  $\text{CH}_2\text{F}-\text{CH}_2\text{F}$  isolated in Ar. Dashed line: before irradiation. Solid line: after 60 sec of irradiation at  $1047.46\text{ cm}^{-1}$  with an intensity of  $10\text{ mW/cm}^2$ . A persistent spectral hole is produced by the laser light. ( After Ref. [6.4])

Figure 6.3 Temperature dependence of the hole linewidth of the matrix split  $\nu_{17}$  mode in *trans* DFE:Kr. The crosses identify the experimental points which have been taken at short irradiation time and have been corrected for the laser linewidth. The lines identify phonon induced vibrational dephasing as given by the Raman mechanism: Solid curve, Debye model with  $\theta_D = 38\text{ K}$ ; Dot-dash, Debye model with  $\theta_D(\text{Kr}) = 72\text{ K}$ ; Dotted, Einstein model with  $\theta_E = 35\text{ K}$ . (After Ref. [6.6])

Figure 6.4 Polarization properties of holes in the matrix split  $\nu_{17}$  mode in *trans* DFE:Kr. The top trace shows the spectrum before irradiation. A hole is burned at one frequency with the polarization vertical (V) and at a second with the polarization horizontal (H). The spectra are then recorded with the two polarizations (V) and (H) as shown. (After Ref. [6.4])

Figure 6.5 Spectra demonstrating IR induced interconversion of *gauche* and *trans* DFE:Xe. (a) Solid line: immediately after deposition, dashed line: after 90 min exposure to unfiltered globar source; (b) sample exposed during deposition and for 120 min to give photostationary



trace, "g" and "t" stand for *gauche* and *trans*, respectively; (c) Solid line: after 100 min CO<sub>2</sub> laser radiation (9P(22) at 130 mW/cm<sup>2</sup>), dashed line: (b) spectrum after irradiation. (After Ref. [6.51])

Figure 6.6 Diode laser transmission spectrum of 0.2 cm thick KI + 0.001 mole % KReO<sub>4</sub><sup>-</sup> at 2K. The 10P(42) absorption of hot CO<sub>2</sub> serves as a frequency marker. (after Ref. [6.43])

Figure 6.7 Illustration of incoherent laser saturation measurements for matrix-isolated ReO<sub>4</sub><sup>-</sup> at two different temperatures. Persistent spectral features are observed with very small laser intensities. (after Ref. [6.52])

Figure 6.8 Saturation intensity  $I_s$  versus  $\nu_3$  mode frequency divided by the LA-phonon frequency at the zone boundary. (after Ref. [6.52])

Figure 6.9 Examples of persistent infrared spectral hole growth and erasing. (a) After cooling a sample of RbI + 0.8% KReO<sub>4</sub> from 77 K to 1.4 K in the dark, the CO<sub>2</sub> laser probe beam was unblocked at  $t_1$ . (b) After long exposure to the probe beam, the pump beam is unblocked at  $t_2$ , erasing the probe hole, and blocked again at time  $t_3$ . (after Ref. [6.10])

Figure 6.10 Persistent hole lineshape measurements with two CO<sub>2</sub> lasers for RbI:ReO<sub>4</sub><sup>-</sup>. The initial probe transmissions at  $\Delta f = 20$  and 22.5 MHz were averaged to define  $T_i$ . The open and closed circles correspond to measurements at different sample locations. (after Ref. [6.10])

Figure 6.11 Potential energy diagrams for the  $\text{ReO}_4^-$  spherical-top molecule in the ground and excited  $\nu_3$  mode vibrational states. Two possible configurations A and B occur for each state. (after Ref. [6.10])

Figure 6.12 High resolution spectrum of KI + 0.05 mole %  $\text{KReO}_4$  + 2 mole % NaI showing laser coincidences at  $T = 6$  K.

Figure 6.13 (a) Infrared transmission spectrum of KI + 0.05 mole %  $\text{KReO}_4$  + 2 mole % NaI in the region of the  $\nu_3$  mode. (b) Diode laser first derivative spectrum of the peak at  $\text{N}_2\text{O}$  P17. The central feature corresponds to enhanced absorption. (after Ref. [6.11])

Figure 6.14 Photoinduced reorientation model for  $\text{ReO}_4^-$  in alkali halides. Two possible configurations denoted A(A') and B(B') occur for each zero libration state. Arrangement (1) has the double-well asymmetry of the two ground-state configurations larger than for the two excited states and arrangement (2) has the opposite. The bottom figure shows the line strengths vs frequency for each of the transitions in the two arrangements. (after Ref. [6.11])

Figure 6.15 Ultrasonic absorption peak for three alkali halides doped with  $\text{KReO}_4$ . (after Ref. [6.54])

Figure 6.16 Temperature dependence of the first overtone vibration of  $\text{CN}^-$  in KBr. (after Ref. [6.58])

Figure 6.17 High resolution absorption spectra of  $\text{CN}^-$  in KBr. (a) Impurity induced absorption coefficient in the  $\text{CN}^-$  stretch region for KBr + 0.05 mole % KCN. The vertical dashed line

divides the spectrum into two parts: right, isotope lines of  $\text{NCO}^-$ ; left, lines of  $\text{CN}^-$ . The center frequencies are recorded in Table 6.2. (b) Expanded view of the  $\text{CN}^-$  region for a 0.01 mole % dopant concentration. Hole burning has been observed on the lines  $\alpha_1$ ,  $\alpha_2$ ,  $\gamma_1$ ,  $\gamma_2$ ,  $\gamma_3$ , and  $\gamma_4$ . The sample temperature is 1.7 K and the FTIR resolution is  $0.04 \text{ cm}^{-1}$ . (after Ref. [6.13])

Figure 6.18 Three examples of persistent hole burning spectra. Each case shows both before and after burning: (a)  $\alpha_1$  band, (b)  $\alpha_2$  band, and (c)  $\gamma_1$  band. All holes are power broadened. Sample temperature is 1.7 K. (after Ref. [6.13])

Figure 6.19 Stability of the persistent holes in the  $\gamma_1$  band. The temperature is cycled from 1.7 K up to 35 K and back down. The temperatures for the four cases shown are: (a) 1.7 K, (b) 15 K, (c) 25 K, (d) 35 K and (e) back to 12.7 K again. (after Ref. [6.13])

Figure 6.20 Vibrational emission spectrum of  $\text{CN}^-$  in KBr. The concentration is 0.12 mole % KCN + 0.2 mole % NaBr. (after Ref. [6.13])

Figure 6.21 Polarized hole burning study of the  $\gamma_1$  band. Top: Before and after a hole is burned with probe laser polarization parallel to burn polarization. Bottom: Probe perpendicular to burn polarization. The burn polarization is along the [100] axis. Sample temperature is 1.7 K. (after Ref. [6.12])

Figure 6.22 Milling and erasing the  $\gamma_1$  band. (a) Sweeping the diode frequency over a fixed frequency interval (arrow width) mills a slot. (b) Sweeping the diode frequency over 4 GHz for 80 min erases the entire  $\gamma_1$  band. (after Ref. [6.13])

Figure 6.23 Identification of the persistent hole product state,  $\gamma_1'$ . Top: The FTIR spectrum before hole burning on the  $\gamma_1$  band. Bottom: FTIR difference spectrum after most of the  $\gamma_1$  band is erased by the diode. The product state,  $\gamma_1'$ , has the same polarization as the hole burned in the  $\gamma_1$  band. FTIR resolution is  $0.04 \text{ cm}^{-1}$  and the sample temperature is 1.7 K. (after Ref. [6.13])

Figure 6.24 Two-configuration diagram for the  $\gamma_1$  and  $\gamma_1'$  centers. The measured energies are  $\gamma_1 = 2071.83 \text{ cm}^{-1}$ ,  $\gamma_1' = 2077.75 \text{ cm}^{-1}$ ,  $V = 1040 \text{ cm}^{-1}$  and  $\epsilon = 104 \text{ cm}^{-1}$ . (after Ref. [6.13])

Figure 6.25 Influence of alkali ion impurities on  $\text{CN}^-$  vibrational spectrum in KBr. (a) 0.12 mole % KCN + 0.2 mole % NaBr. The labeled lines involve the  $\text{Na}^+$  ion and the unmarked ones are either pair modes or  $\text{Cl}^-$  perturbed modes (see Table 6.2 for frequencies). (b) 0.12 mole % KCN + 0.2 mole % LiBr. The labeled lines involve the  $\text{Li}^+$  ion. (c) 0.12 mole % KCN + 0.2 mole % RbBr. The labeled line involves the  $\text{Rb}^+$  ion. Sample temperature is 1.7 K and the resolution is  $0.04 \text{ cm}^{-1}$ . (after Ref. [6.13])

Figure 6.26 Spectrum of oxygenated  $\text{CN}^-$  complexes in KCl (a) before diffusion of oxygen (b) after diffusion. (after Ref. [6.71])

Figure 6.27 Vibrational energy level diagram of  $\text{ReO}_4^-$  and  $\text{BH}_2\text{D}_2^-$  at low frequencies. The three-fold degenerate  $\nu_4$  mode of  $\text{ReO}_4^-$  which is important in the anharmonic decay of the three-fold degenerate  $\nu_3$  mode is indicated. The  $\text{BH}_2\text{D}_2^-$  modes are nondegenerate. The arrows identify the  $\text{CO}_2$  laser frequency used in the saturation experiment.

Table 6. 1 Measured vibrational relaxation times for the  $\nu_3$  mode for  $\text{ReO}_4^-$  in alkali halide lattices ( $T < 10\text{ K}$ )

Host	RbI	KI	KI	KI	RbBr	KBr	RbCl	NaI	KCl
$\text{ReO}_4^-$ (mole %)	0.8	0.005	0.05	0.05	0.05	0.3	0.1	0.2	0.3
Other (mole %)	0.8 $\text{K}^+$	2.5 $\text{Rb}^+$	0.2 $\text{Cs}^+$	2 $\text{Na}^+$	0.05 $\text{K}^+$	2.5 $\text{Rb}^+$	0.1 $\text{K}^+$	0.2 $\text{K}^+$	2.2 $\text{Rb}^+$
$\bar{\nu}_3(\text{cm}^{-1})$	922.9 P(42)	922.9 P(42)			927.0 P(38)	931.0 P(34)	933.0 P(32)	938.7 P(26)	939.0 P(26)
Lattice constant $a$ ( $\text{\AA}$ )	7.34	7.07			6.85	6.60	6.58	6.47	6.29
$I_s$ ( $\text{W}/\text{cm}^2$ )	$0.9 \pm 0.2$	$3.6 \pm 0.8$	$6.8 \pm 1.4$	$3.2 \pm 0.6$	$14 \pm 3$	$53 \pm 10$	$9.3 \pm 2$	$> 700$	$22 \pm 5$
$\alpha_n(\text{cm}^{-1})$ ( $\pm 25\%$ )	0.80	0.13	0.55	0.12	1.1	0.41	1.4		0.1
$T_1 T_2$ ( $10^{-16} \text{ sec}^2$ )	$24 \pm 5$	$6.7 \pm 1.5$	$3.6 \pm 0.8$	$7.6 \pm 1.5$	$1.8 \pm 0.4$	$0.49 \pm 0.09$	$2.9 \pm 0.6$	$< 0.05$	$1.2 \pm 0.3$
$\Delta\nu_{\text{HOM}}$ (MHz, FWHM)	$5.0 \pm 1.5$	$7.8 \pm 0.5$	$9.0 \pm 1.3$	$10 \pm 1.5$	$18 \pm 1.5$	$30 \pm 1.5$	$17 \pm 1.3$		
$T_2$ ( $10^{-8} \text{ sec}$ )	$6.4 \pm 2.0$	$4.1 \pm 0.3$	$3.5 \pm 0.5$	$3.2 \pm 0.5$	$1.8 \pm 0.2$	$1.1 \pm 0.1$	$1.9 \pm 0.2$		
$T_1$ ( $10^{-8} \text{ sec}$ )	$3.8 \pm 1.4$	$1.6 \pm 0.5$	$1.0 \pm 0.3$	$2.4 \pm 0.5$	$1.0 \pm 0.3$	$0.45 \pm 0.15$	$1.5 \pm 0.3$		

Table 6.2 Center frequencies and hole burning properties of the different vibrational modes in the KBr:CN<sup>-</sup> spectrum at 1.7K

<u>Vibrational Center</u>	<u>Frequency (cm<sup>-1</sup>)</u>	<u>Hole burns?</u>
<sup>14</sup> N <sup>12</sup> C <sup>16</sup> O-	2171.57	no
<sup>14</sup> N <sup>12</sup> C <sup>18</sup> O-	2163.45	no
<sup>15</sup> N <sup>12</sup> C <sup>16</sup> O-	2154.23	no
<sup>14</sup> N <sup>13</sup> C <sup>16</sup> O-	2114.43	no
<sup>10</sup> B <sup>16</sup> O <sub>2</sub> -	2030.96	--
<sup>11</sup> B <sup>16</sup> O <sub>2</sub> -	1960.71	--
<sup>12</sup> C <sup>14</sup> N-	2077.60	no
<sup>12</sup> C <sup>15</sup> N-	2045.80	no
<sup>13</sup> C <sup>14</sup> N-	2034.46	no
<sup>12</sup> C <sup>14</sup> N-:Na <sup>+</sup> ( $\gamma_1$ )	2071.83	yes
( $\gamma_1'$ )	2077.75	yes
( $\gamma_2$ )	2076.59	yes
( $\gamma_3$ )	2077.99	yes
( $\gamma_4$ )	2078.22	yes
<sup>12</sup> C <sup>15</sup> N-:Na <sup>+</sup> ( $\gamma_1$ )	2040.22	--
<sup>13</sup> C <sup>14</sup> N-:Na <sup>+</sup> ( $\gamma_1$ )	2028.79	--
<sup>12</sup> C <sup>14</sup> N-:Cl <sup>-</sup> ( $\alpha_1$ )	1076.21	yes
( $\alpha_2$ )	2078.45	yes
<sup>12</sup> C <sup>14</sup> N-:Li <sup>+</sup> ( $\beta_1$ )	2066.81	no
( $\gamma_1$ )	2074.07	no
( $\beta_2$ )	2078.14	no
( $\beta_3$ )	2078.39	--
( $\gamma_1'$ )	2083.57	no
( $\beta_1'$ )	2084.43	--
<sup>12</sup> C <sup>14</sup> N-:Rb <sup>+</sup> ( $\gamma_2$ )	2076.84	no
<sup>12</sup> C <sup>14</sup> N-: <sup>12</sup> C <sup>14</sup> N-	2079.98	no
<sup>12</sup> C <sup>14</sup> N-: <sup>12</sup> C <sup>14</sup> N-	2075.22	no

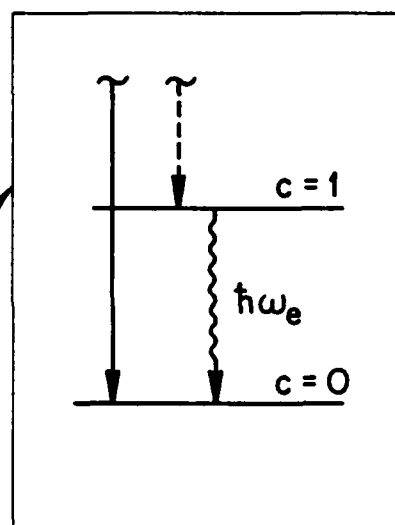
$n = 3$  \_\_\_\_\_

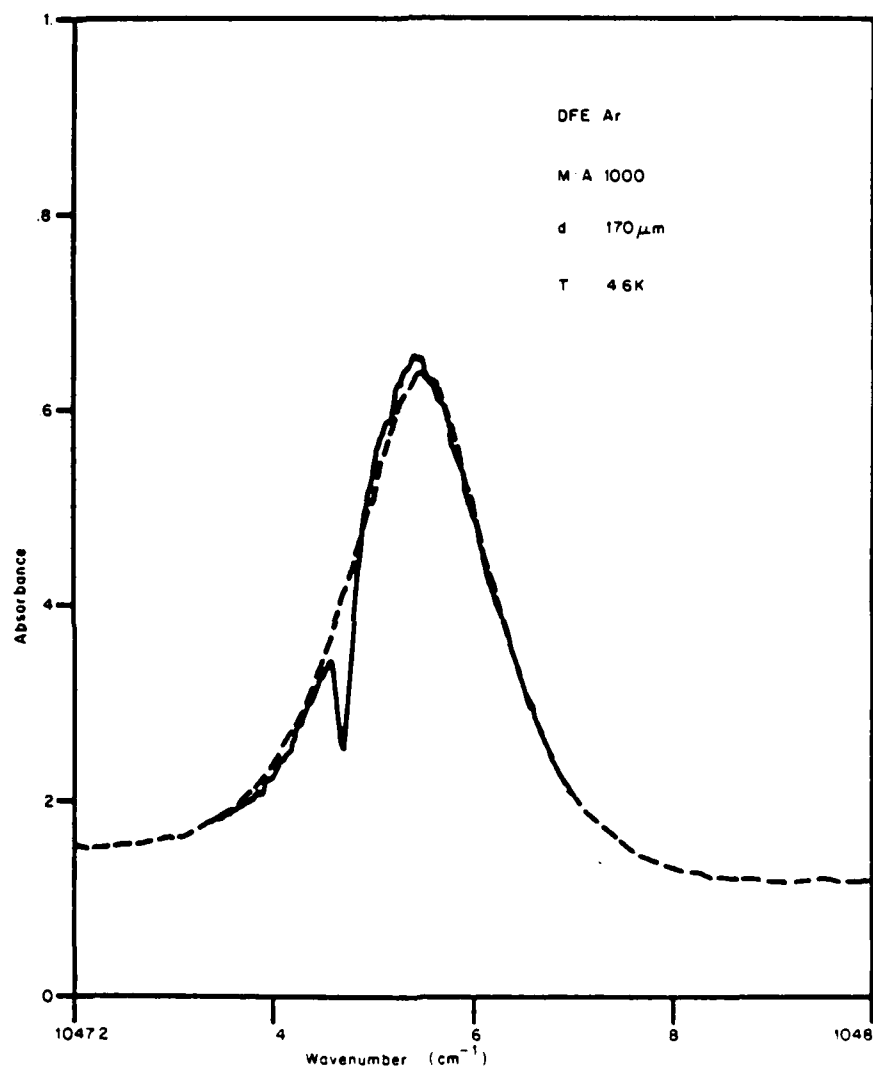
$n = 2$  \_\_\_\_\_

$n = 1$  \_\_\_\_\_

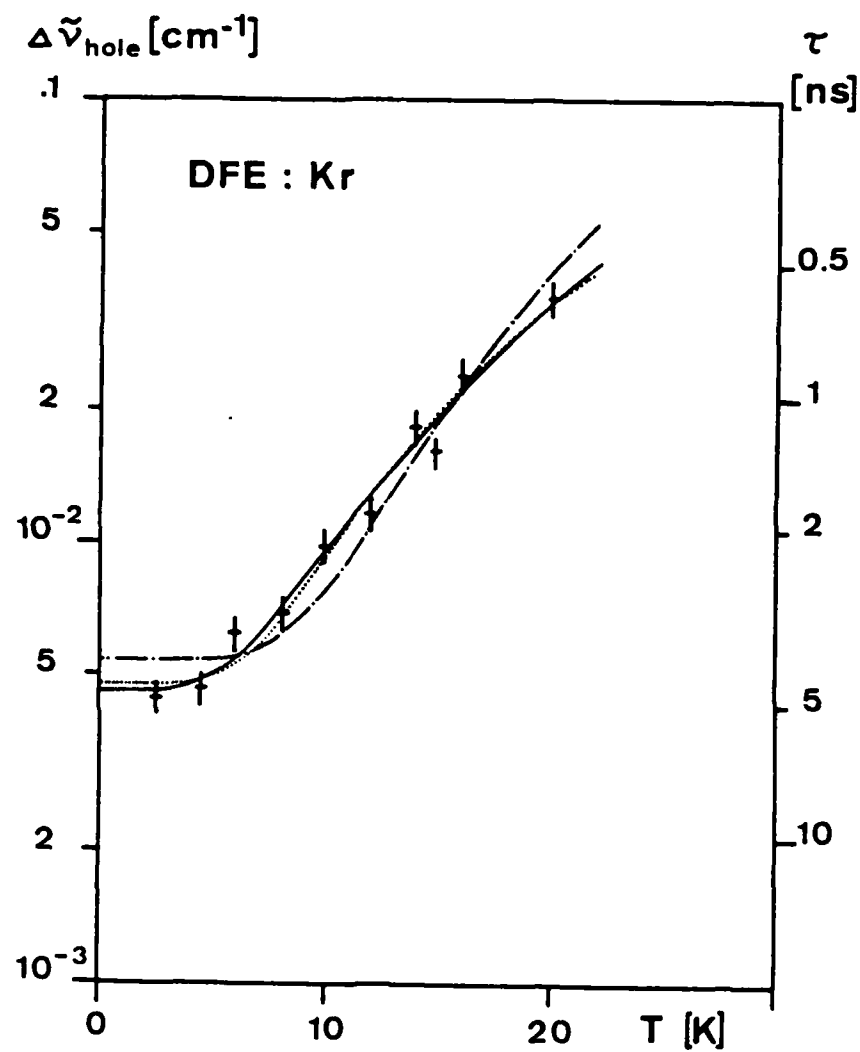
$n = 0$  \_\_\_\_\_

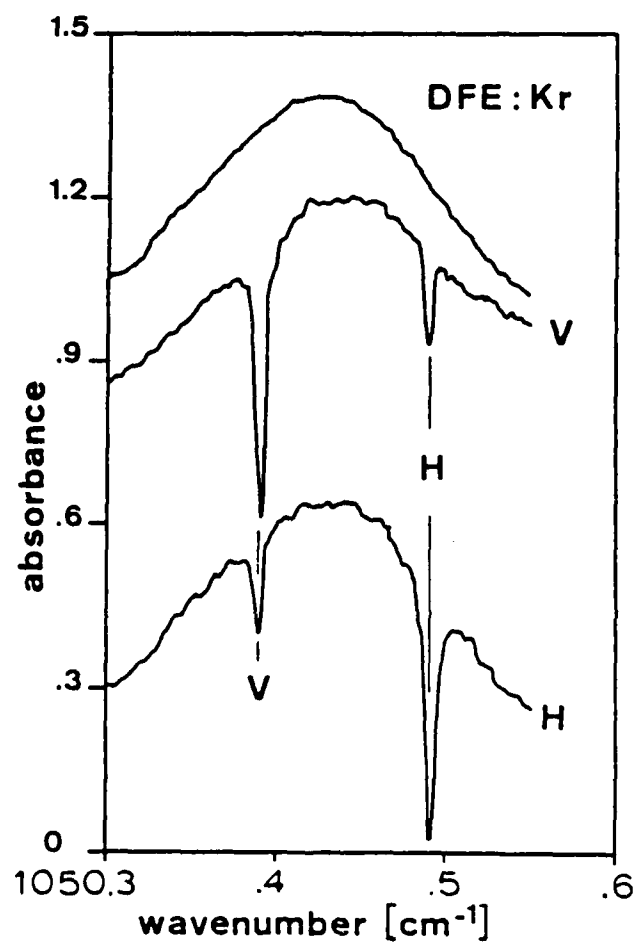
$\hbar\omega_L$

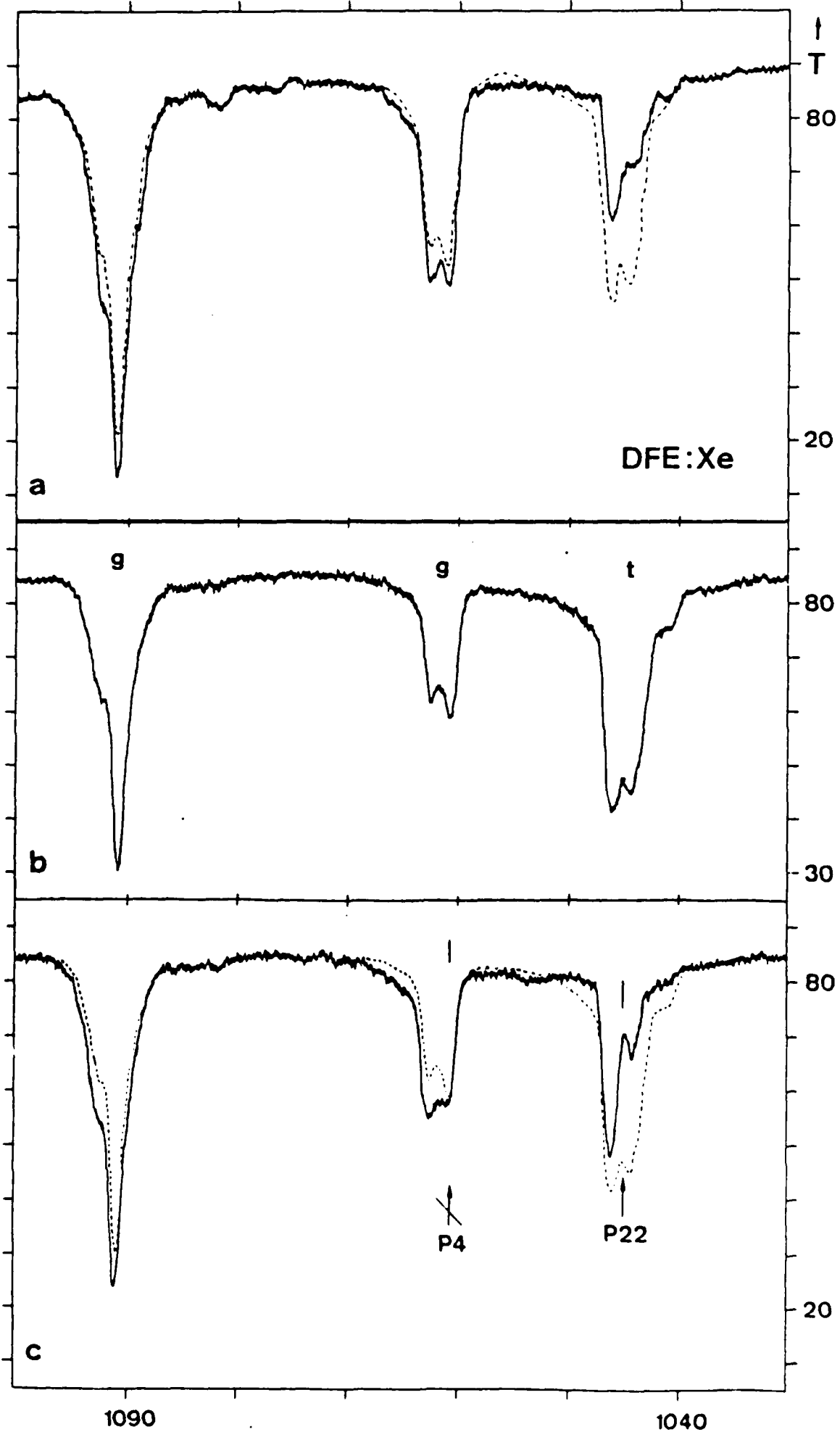


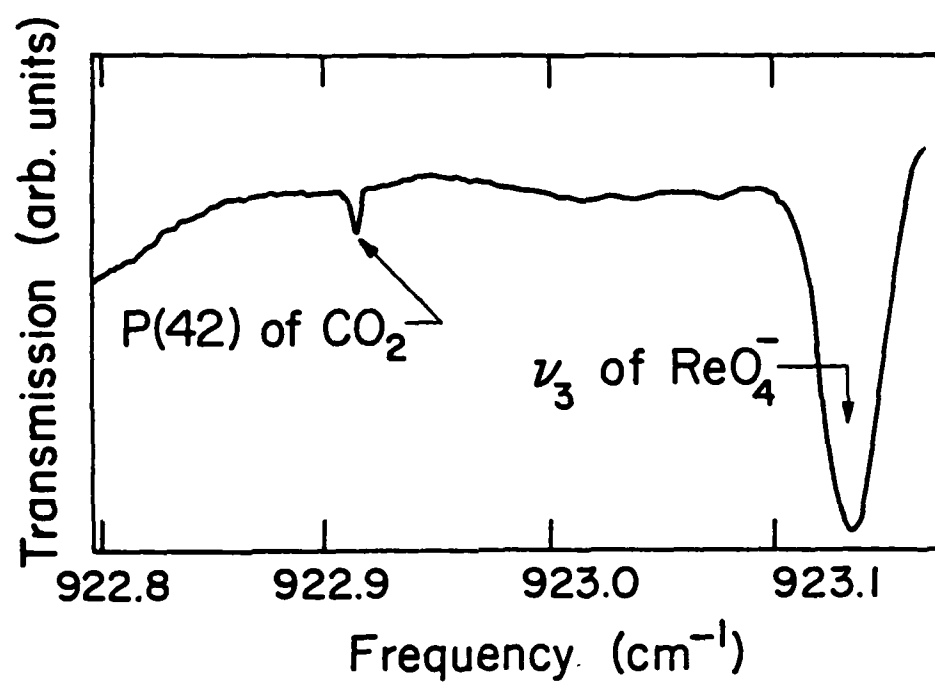


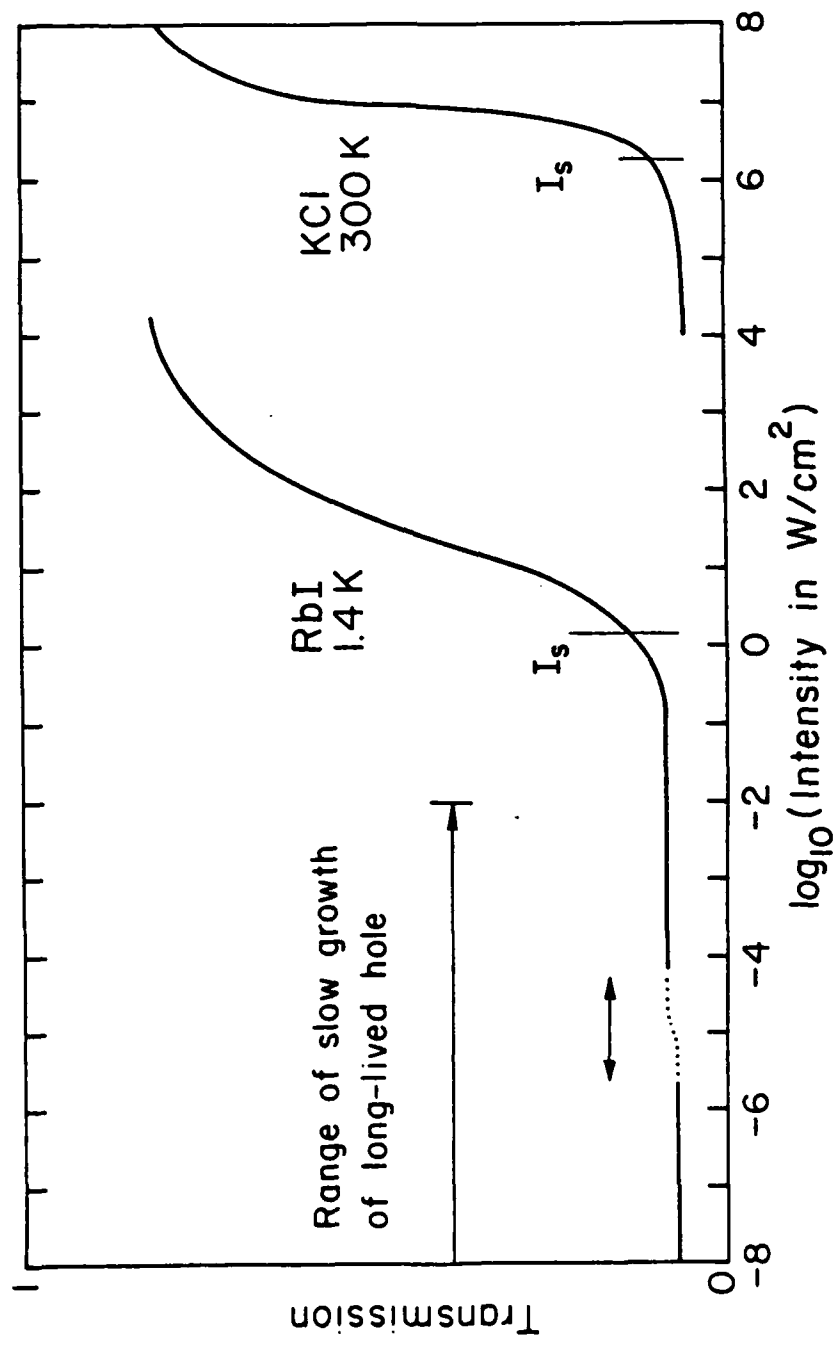


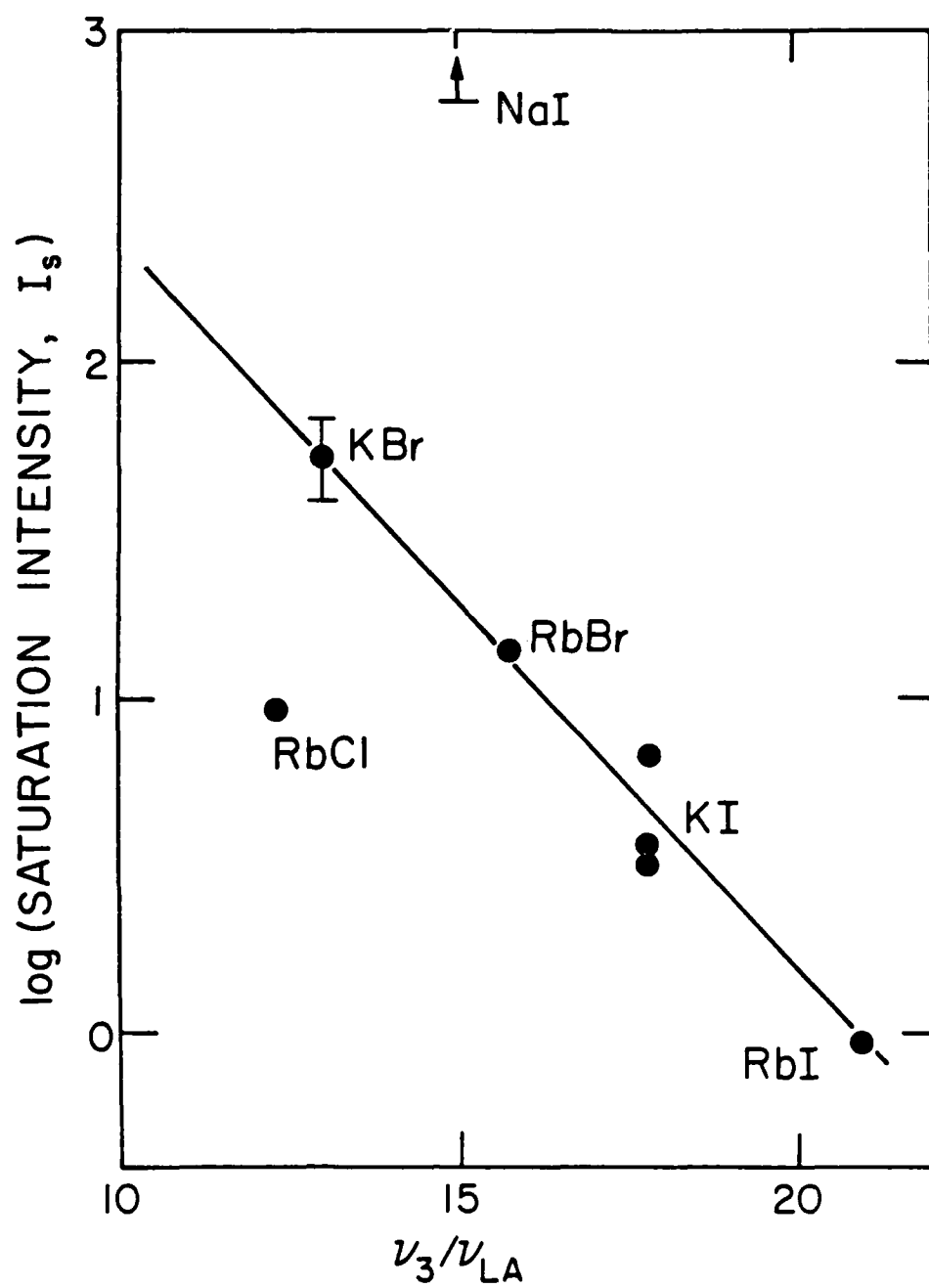


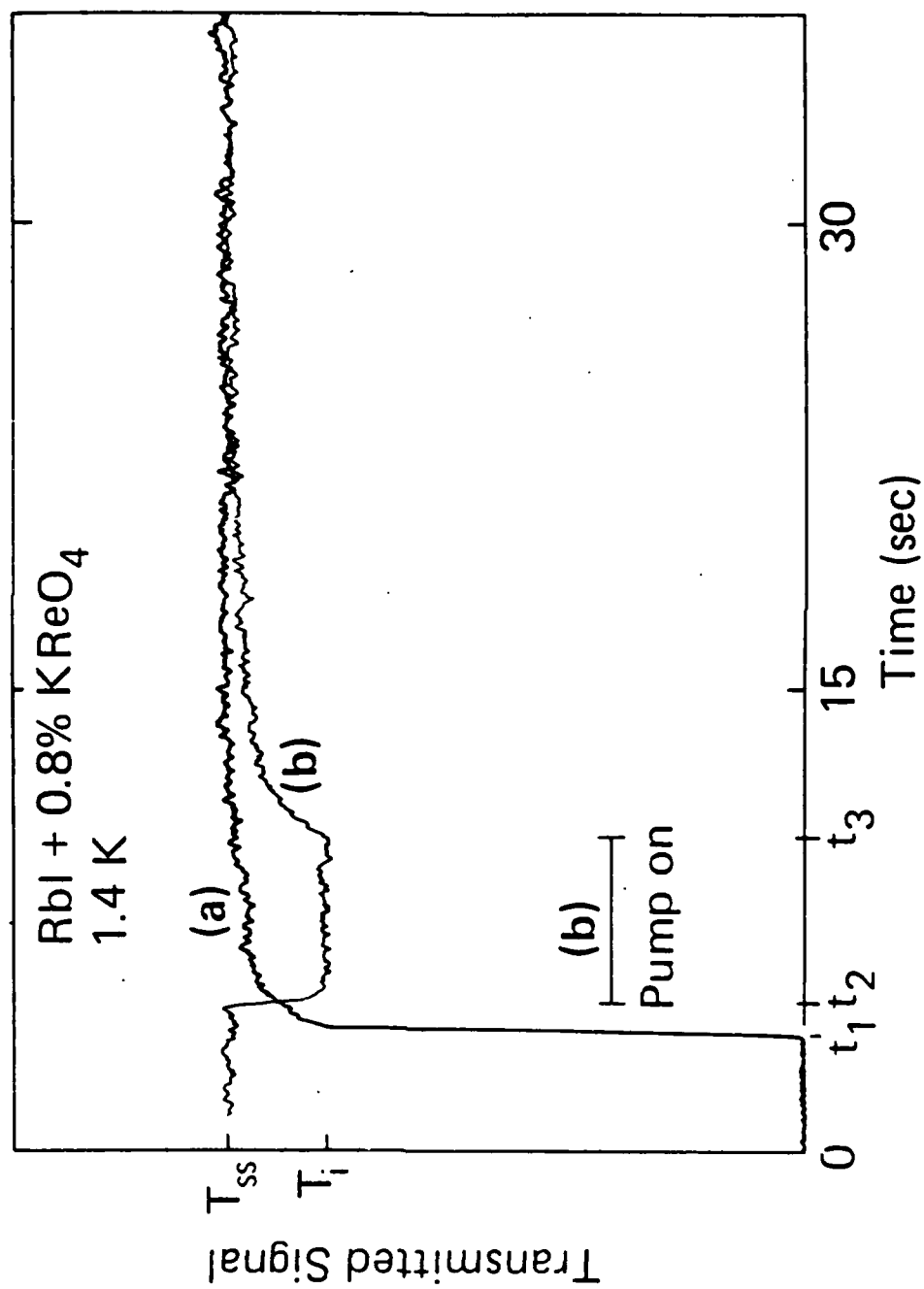


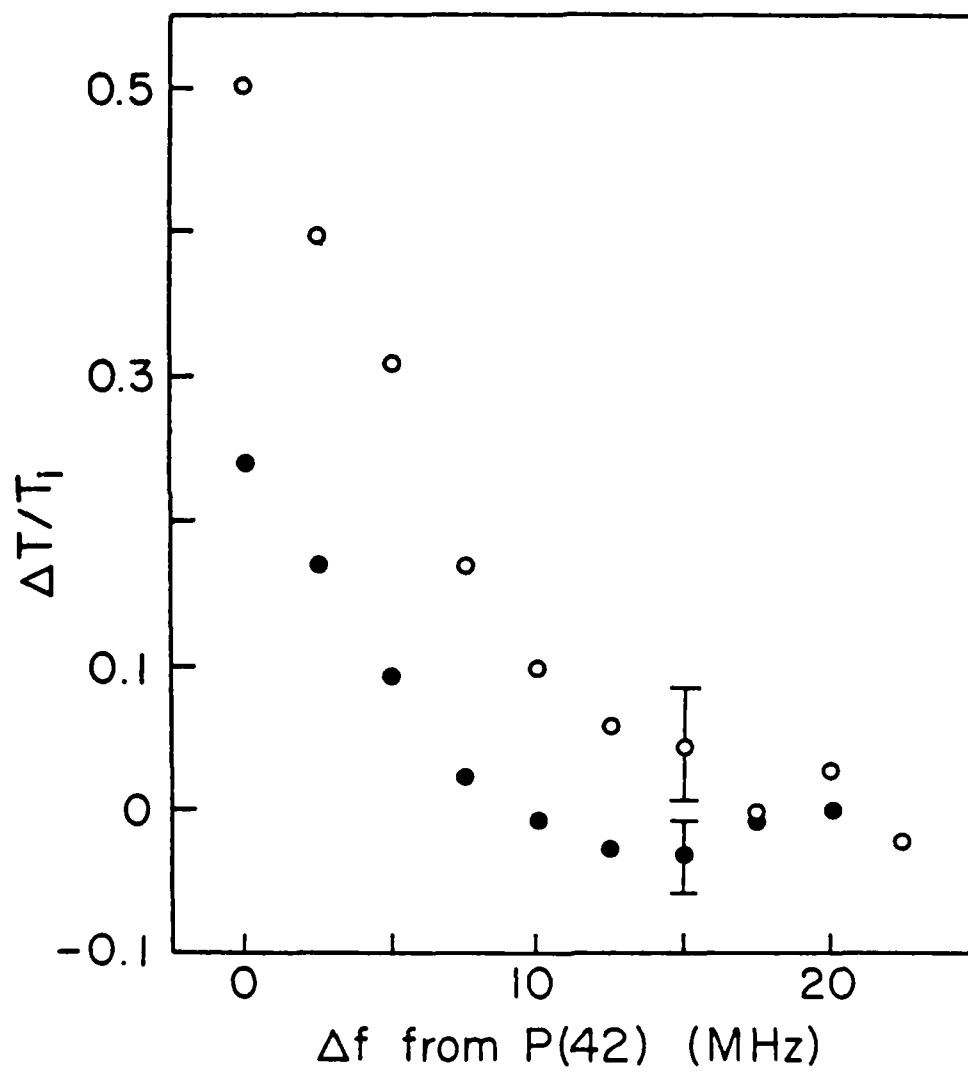




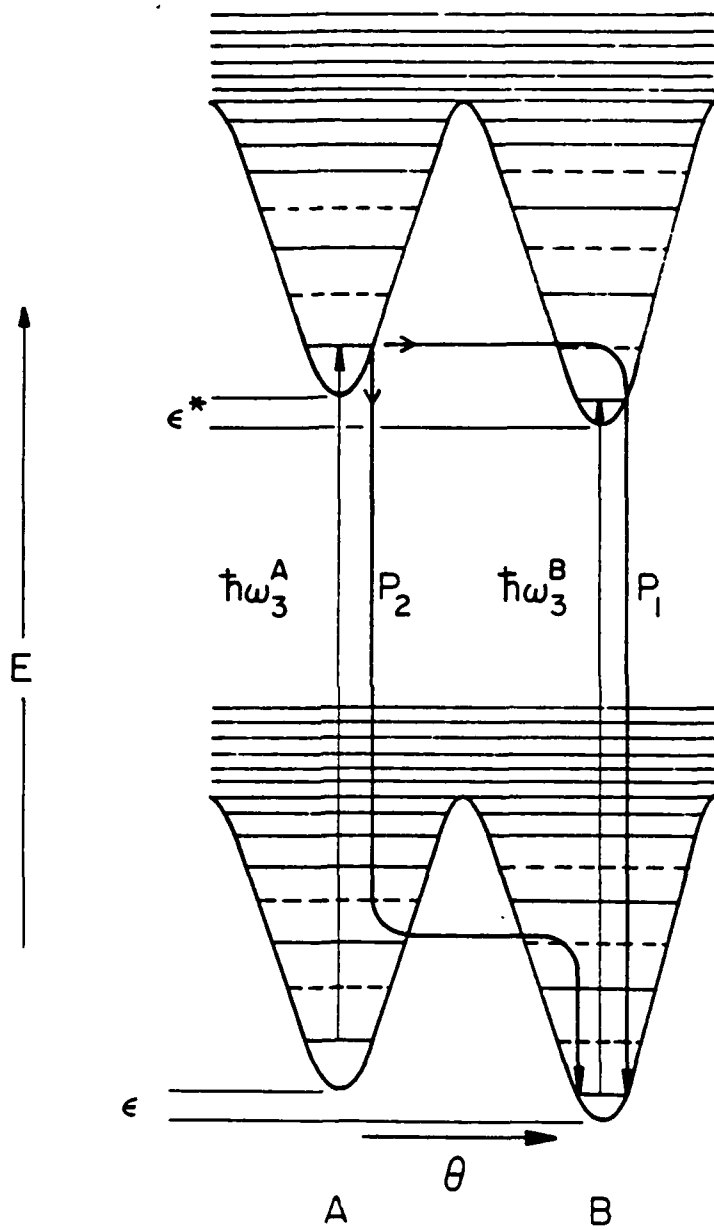


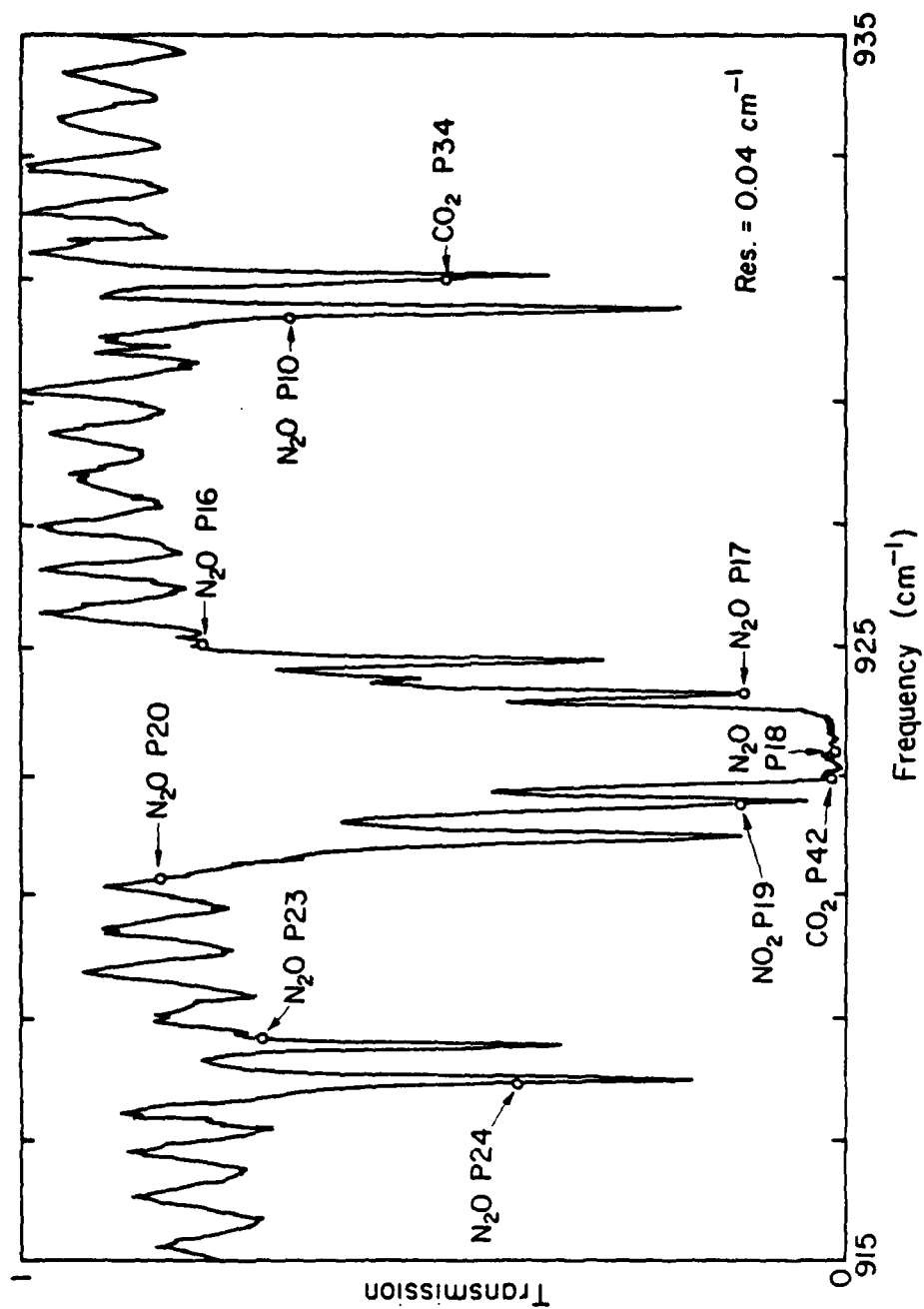


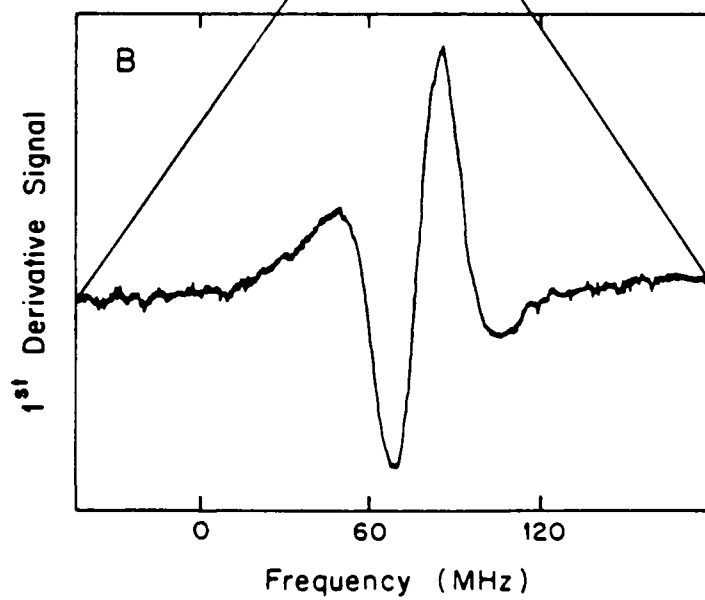
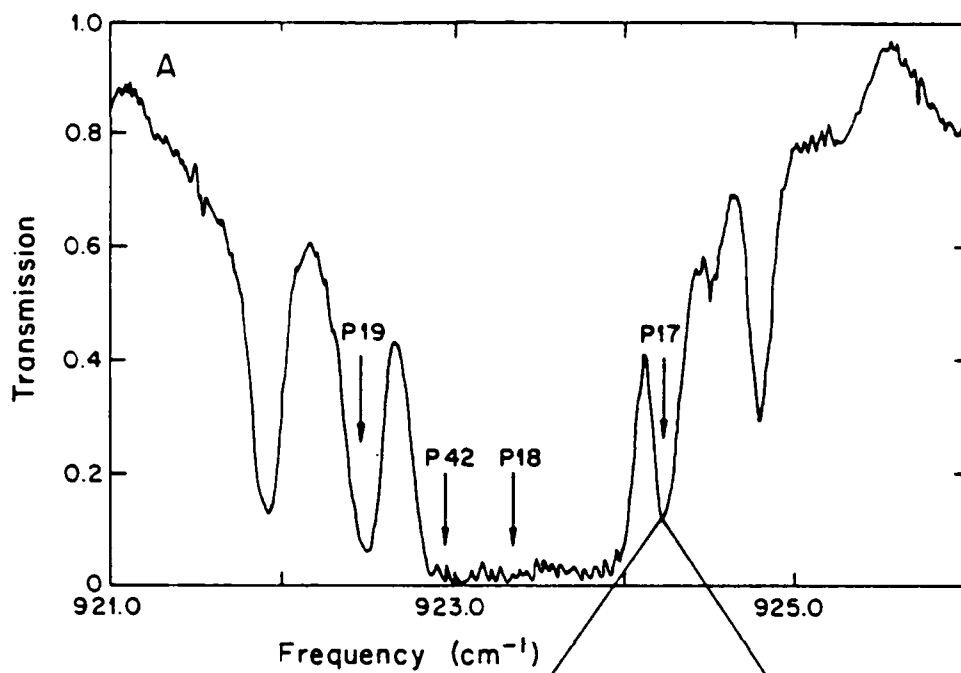


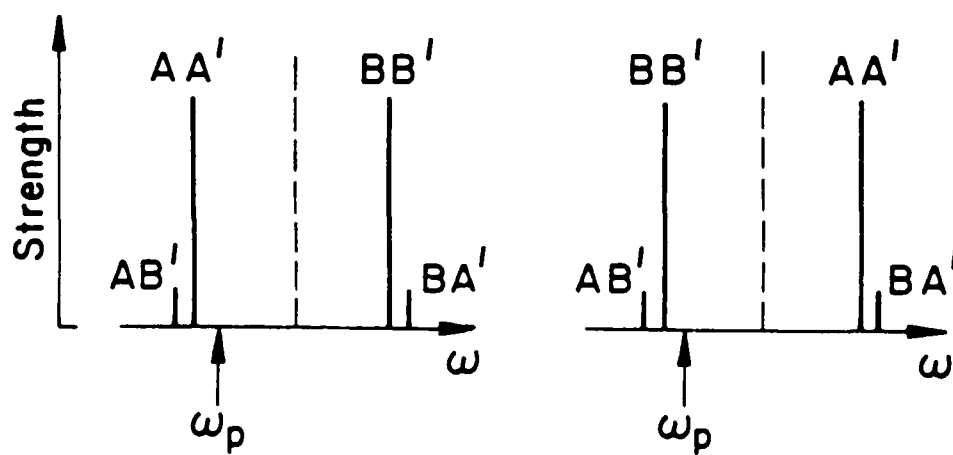
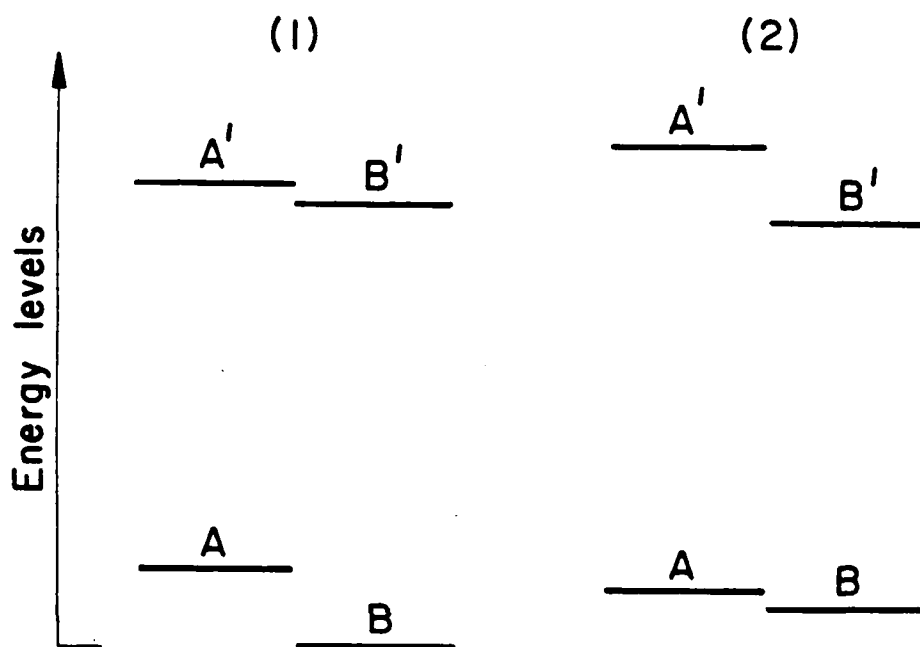


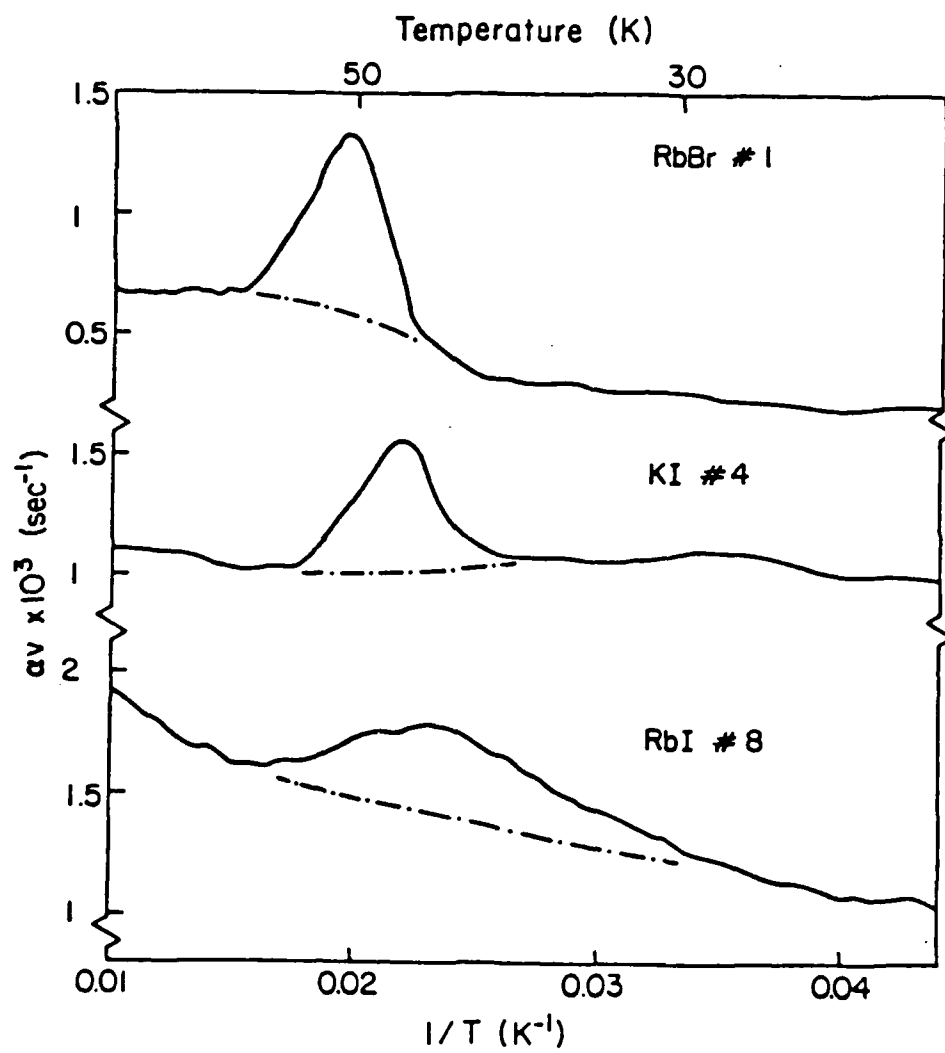


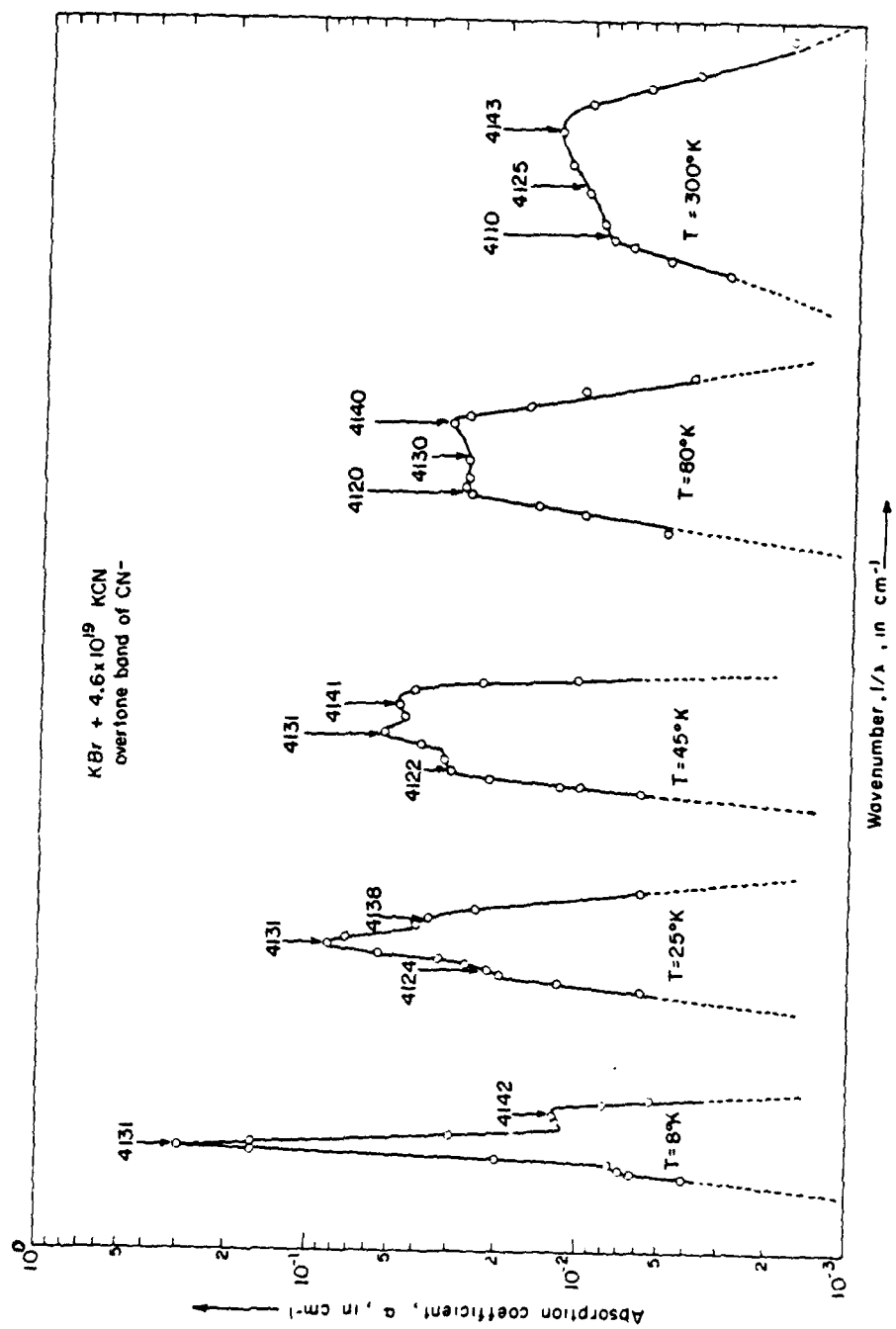


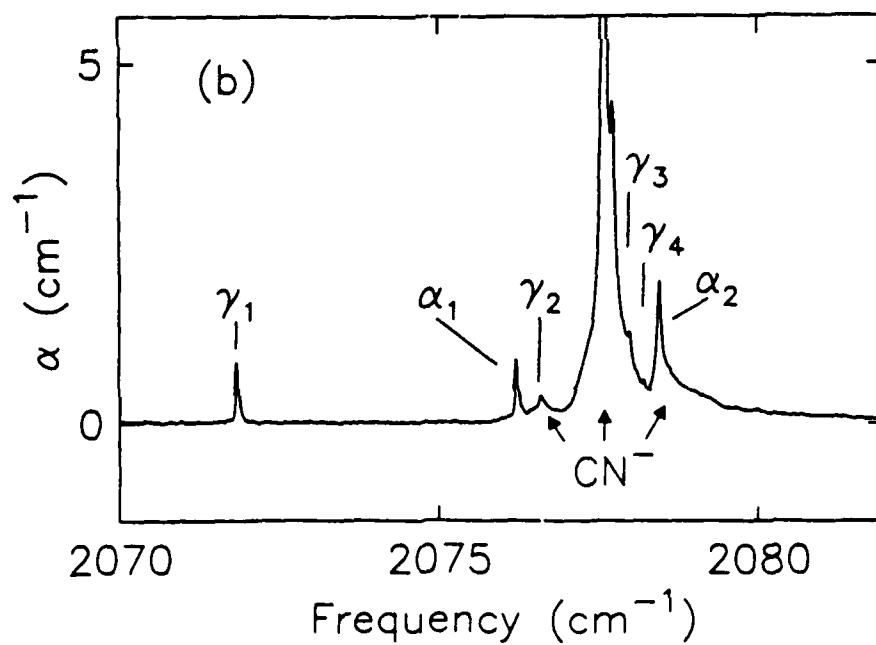
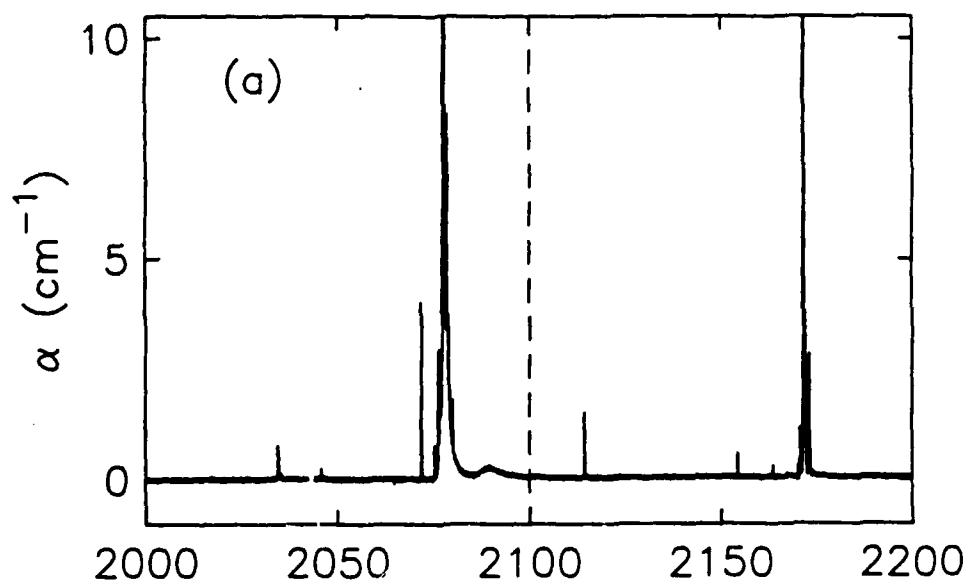


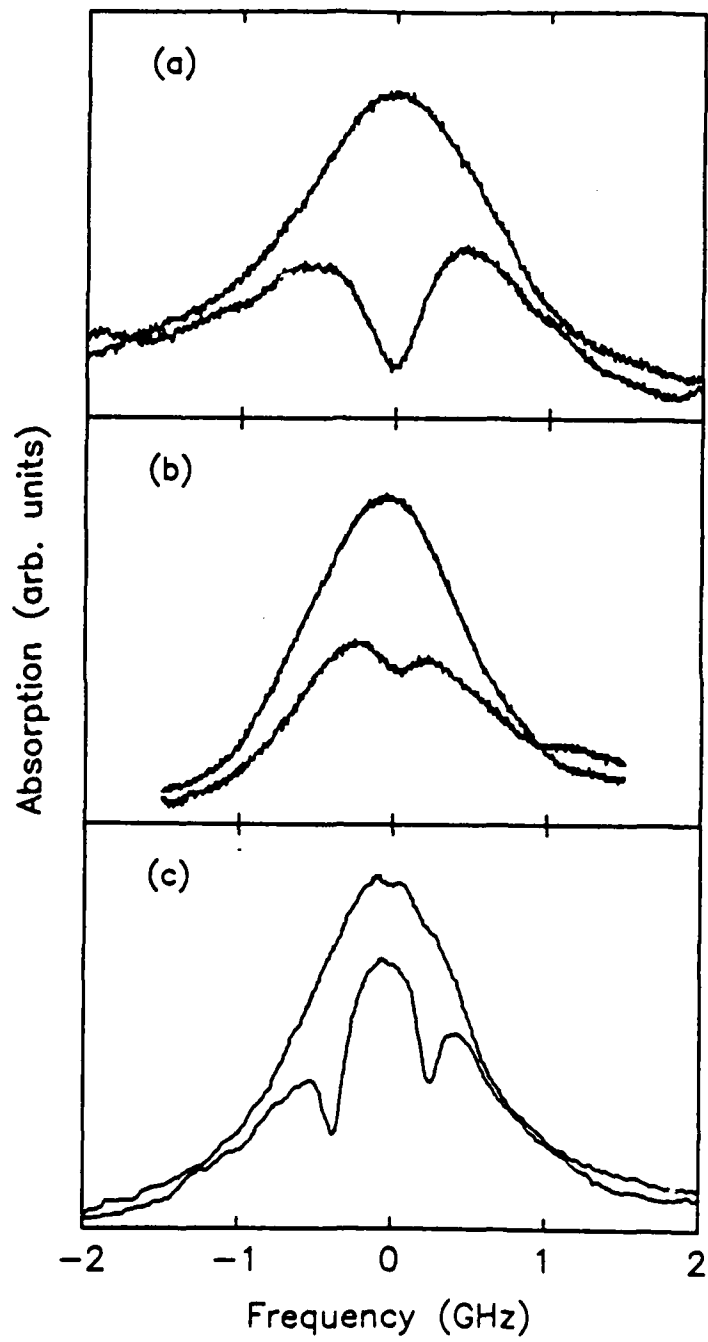




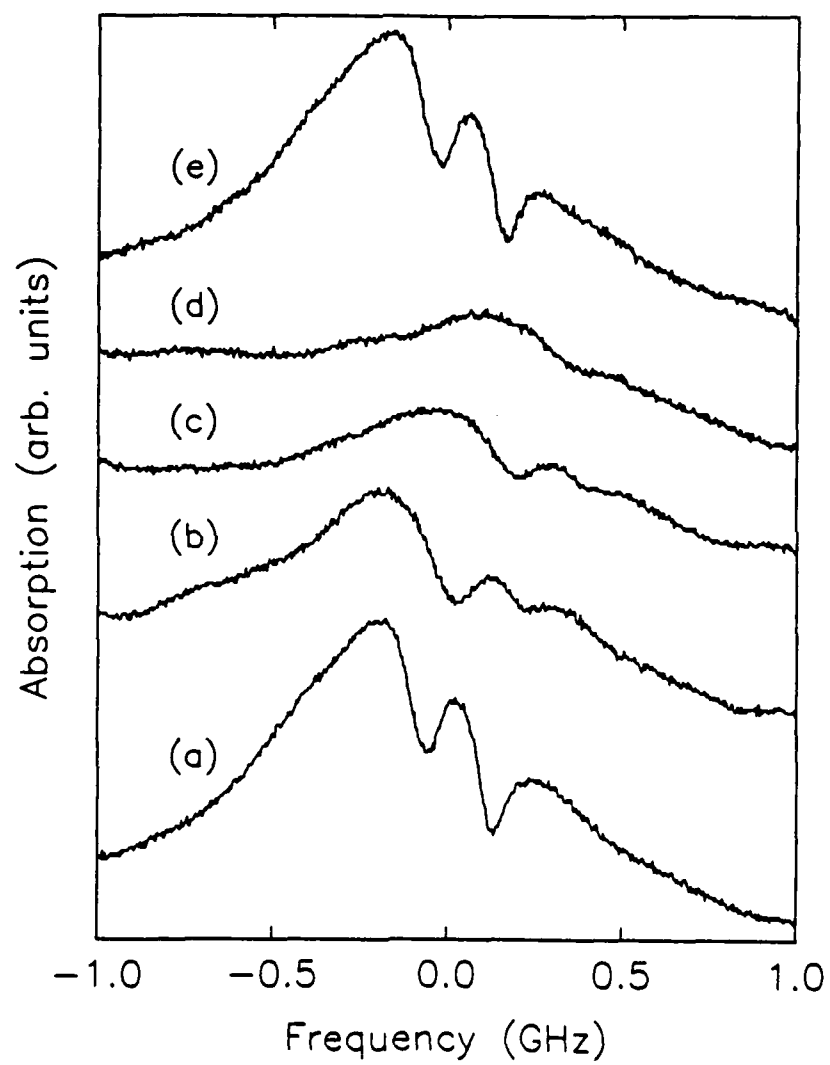


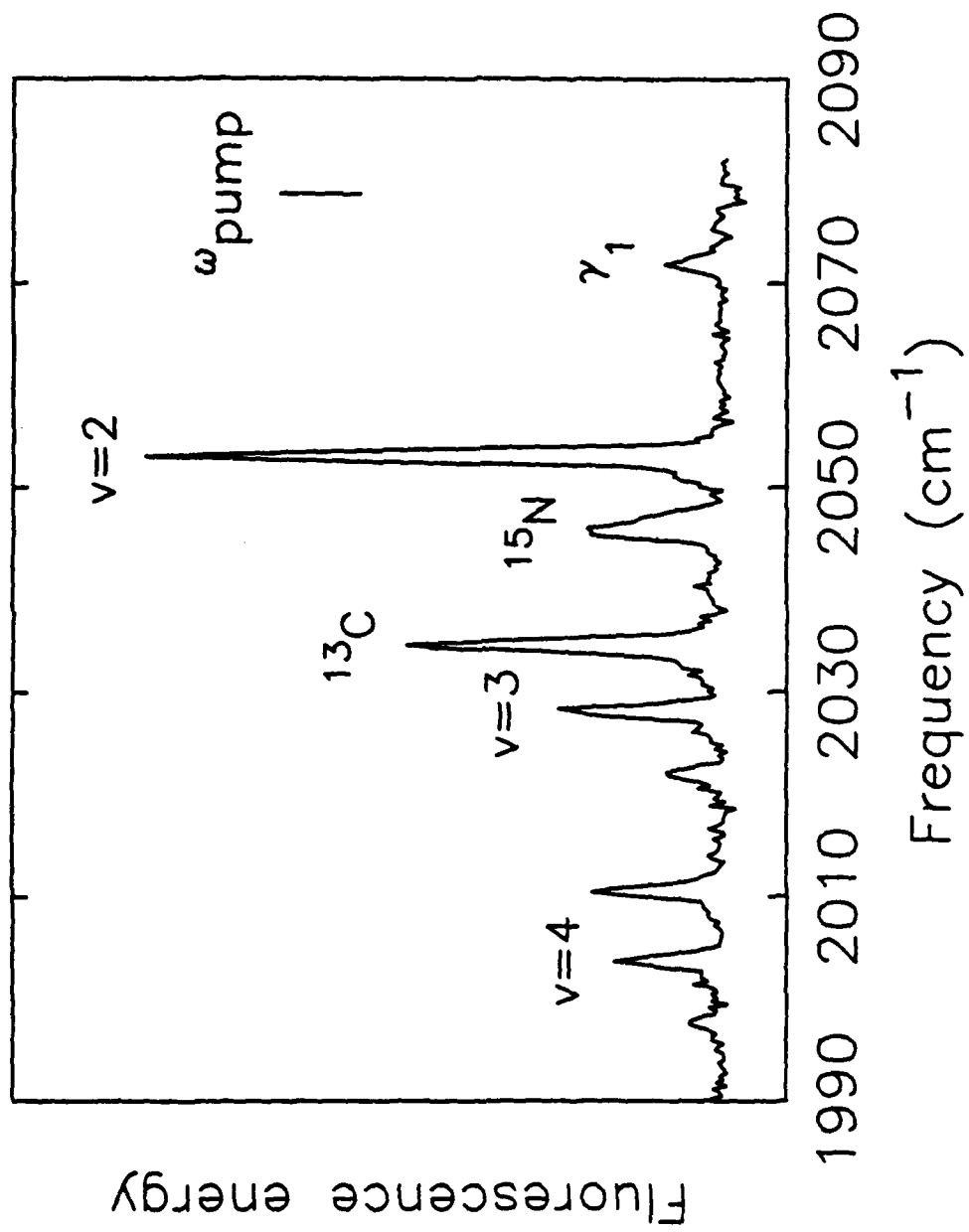


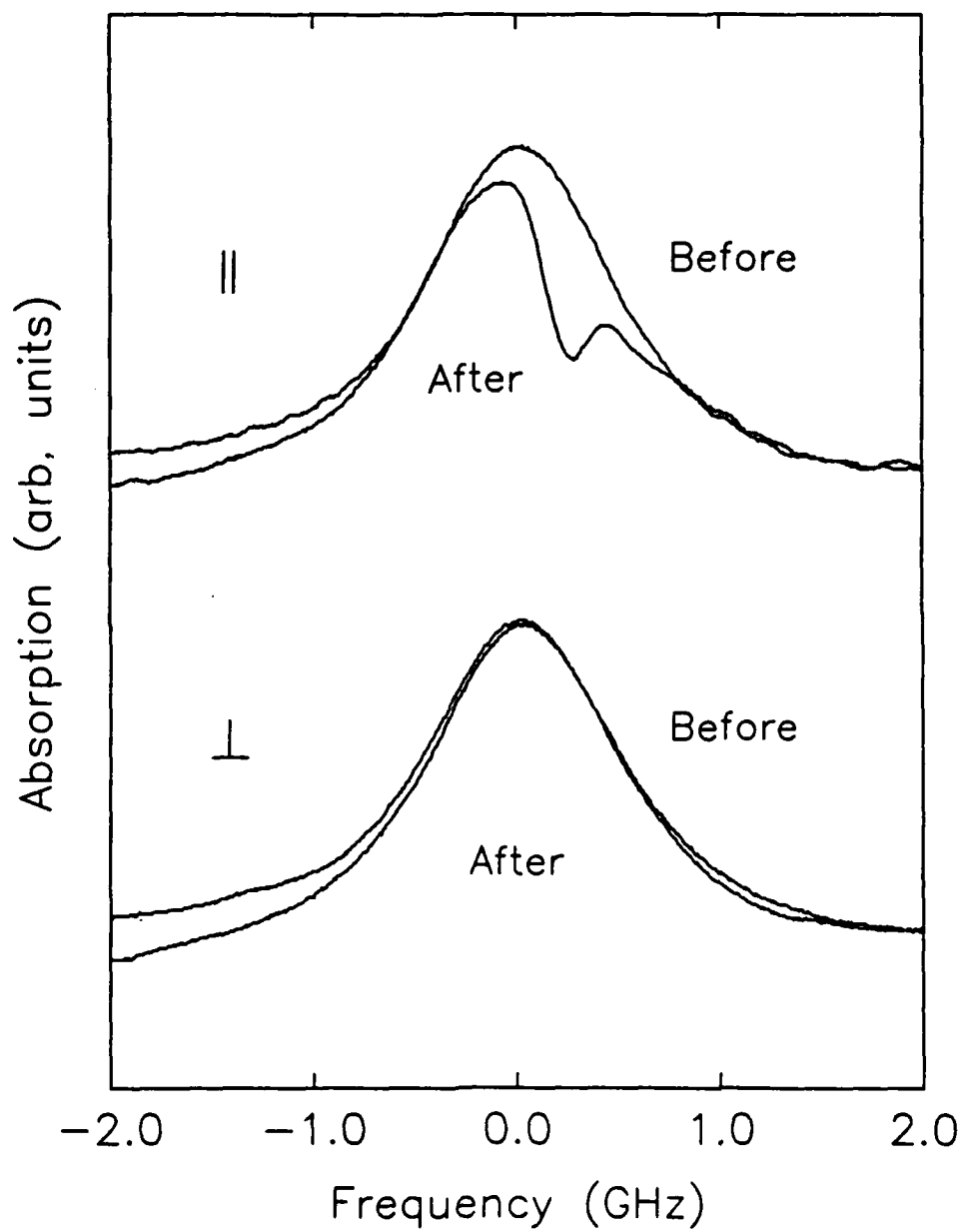


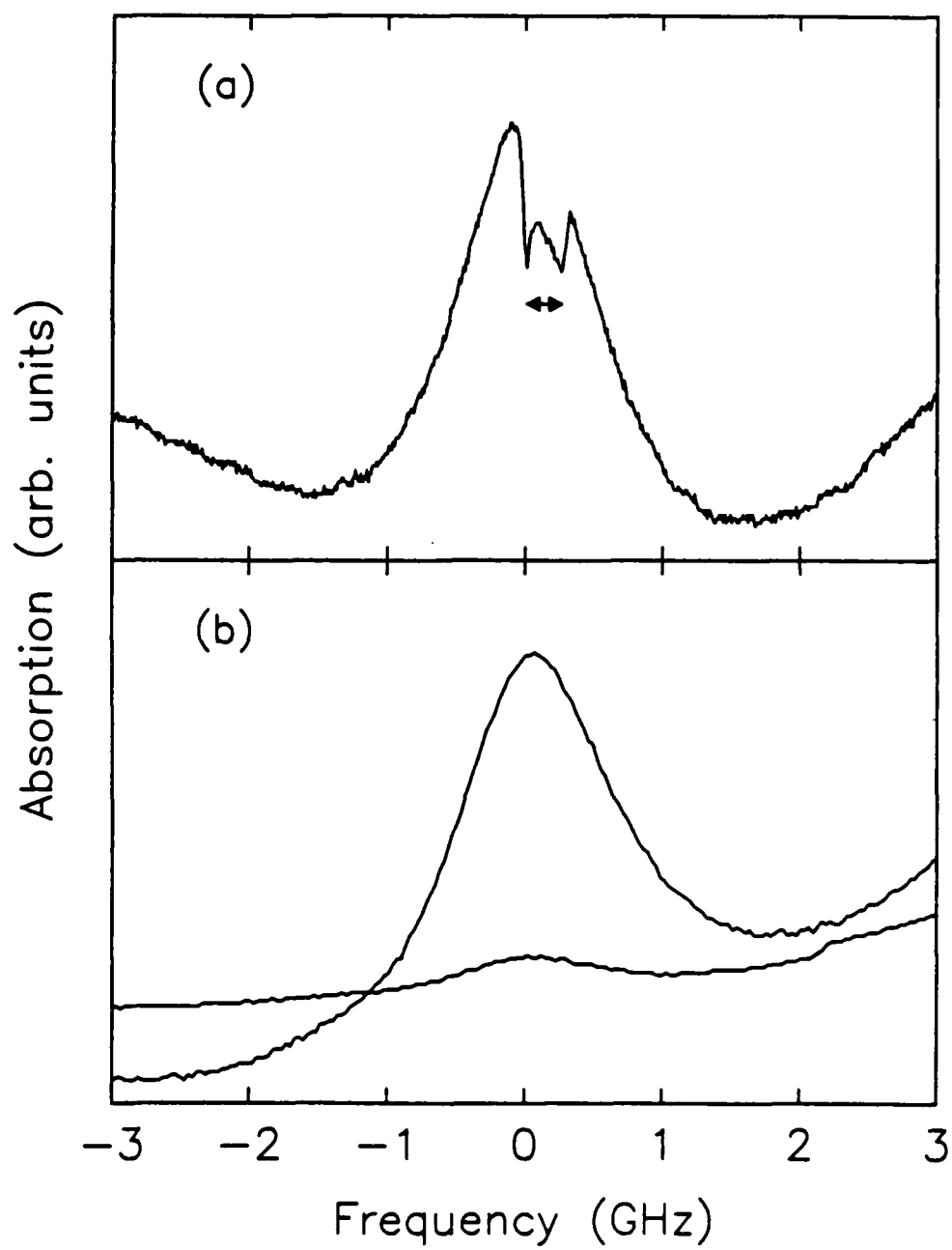


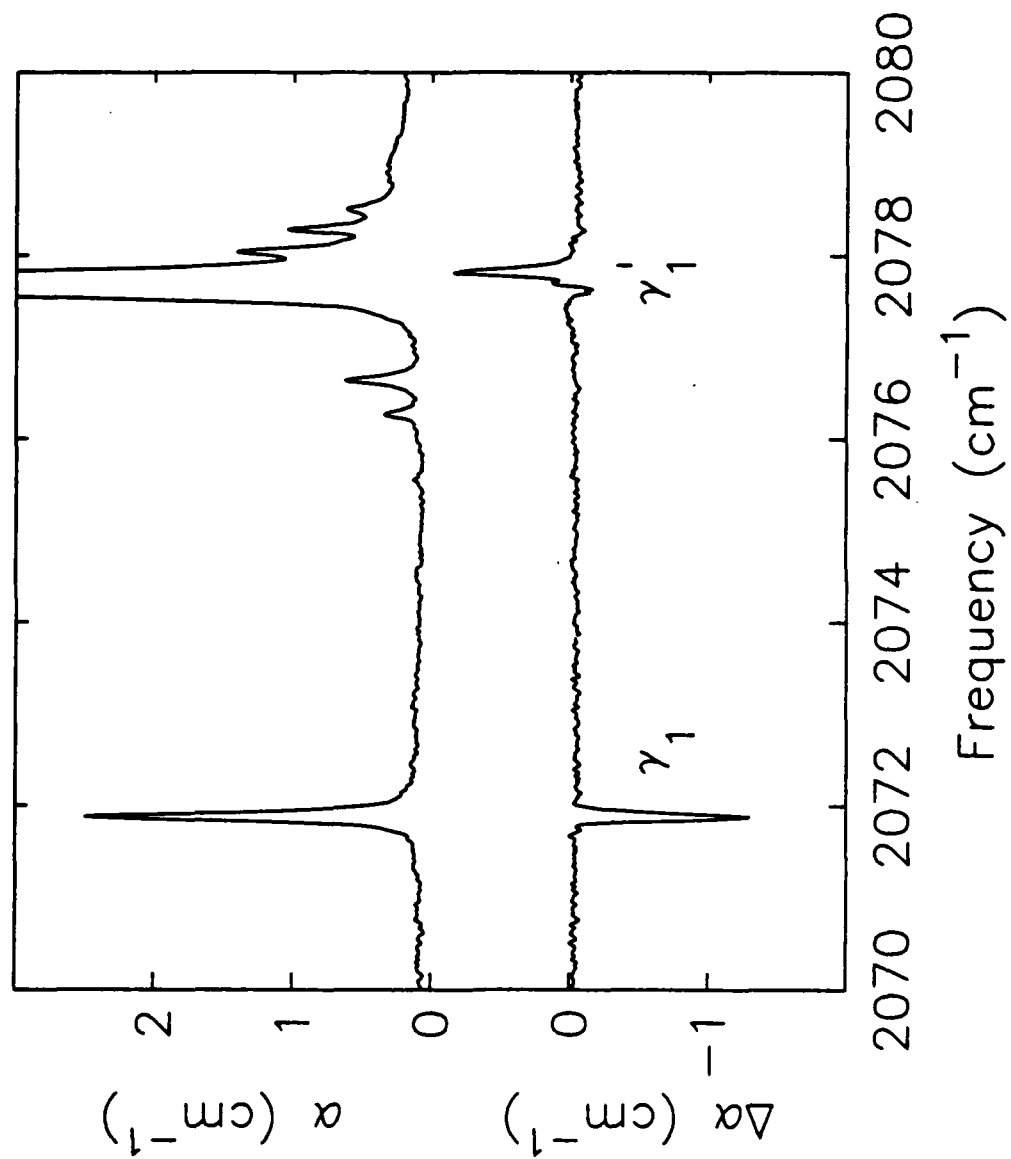


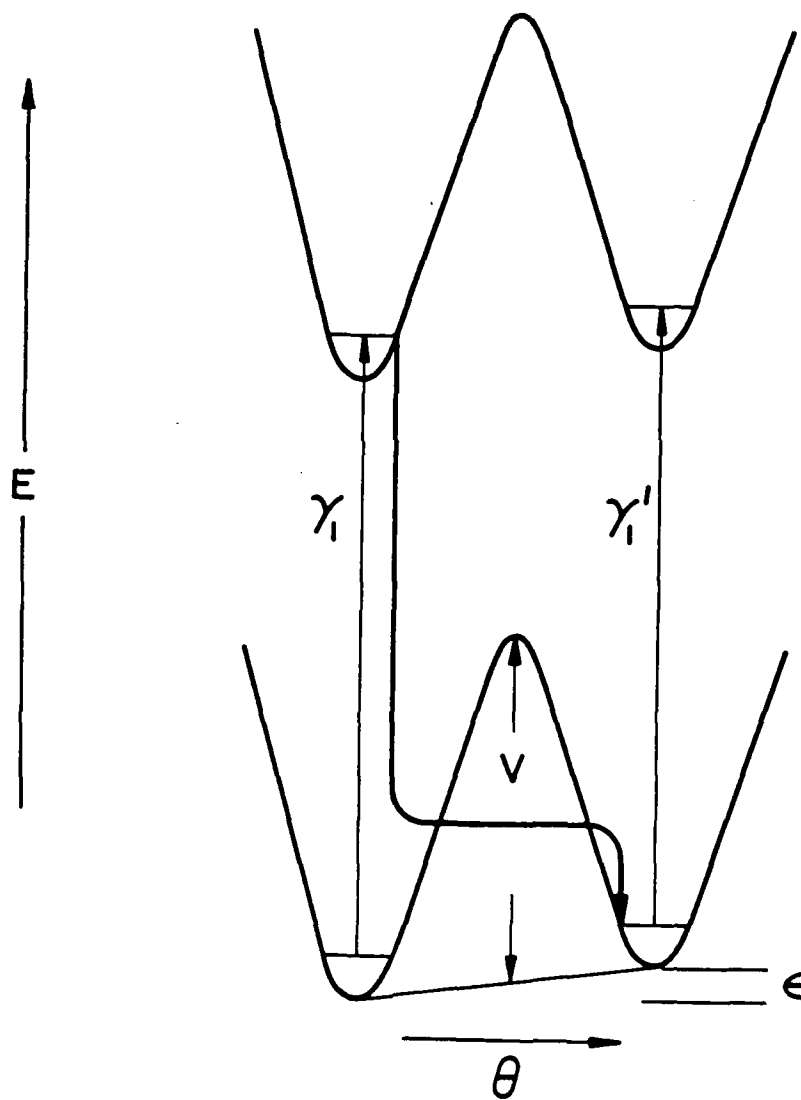
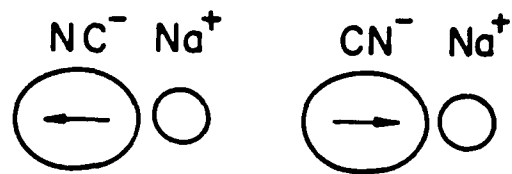


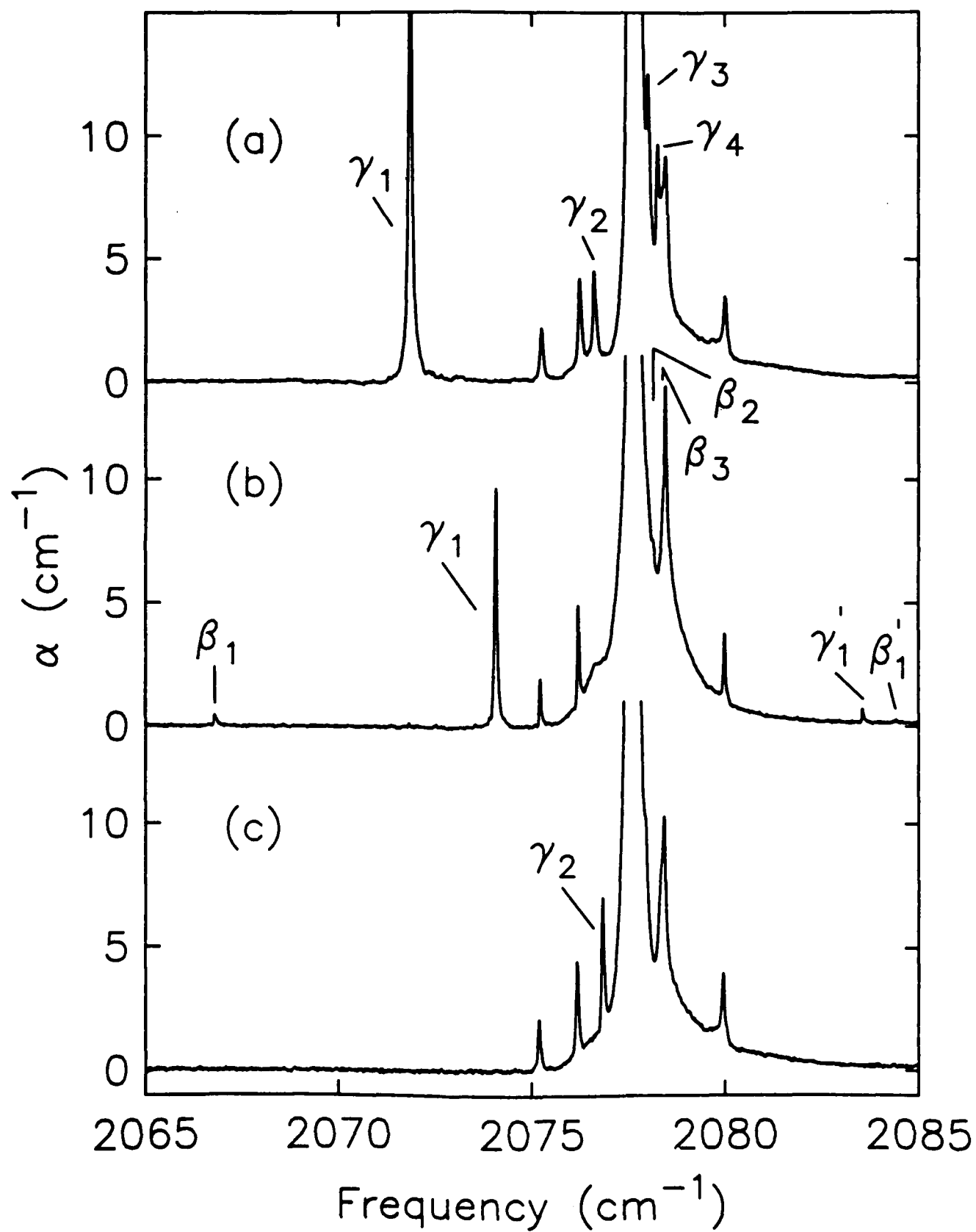












$\nu_3$  —————



$\text{ReO}_4^-$

$\nu_4$  —————

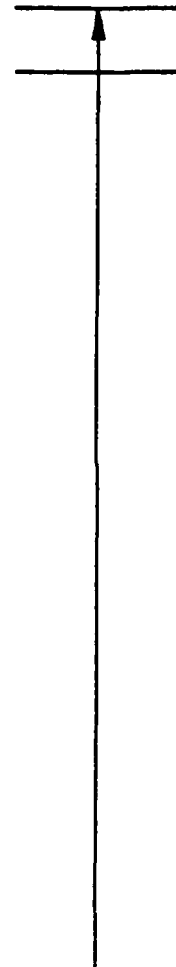


$\nu_4$

a —————

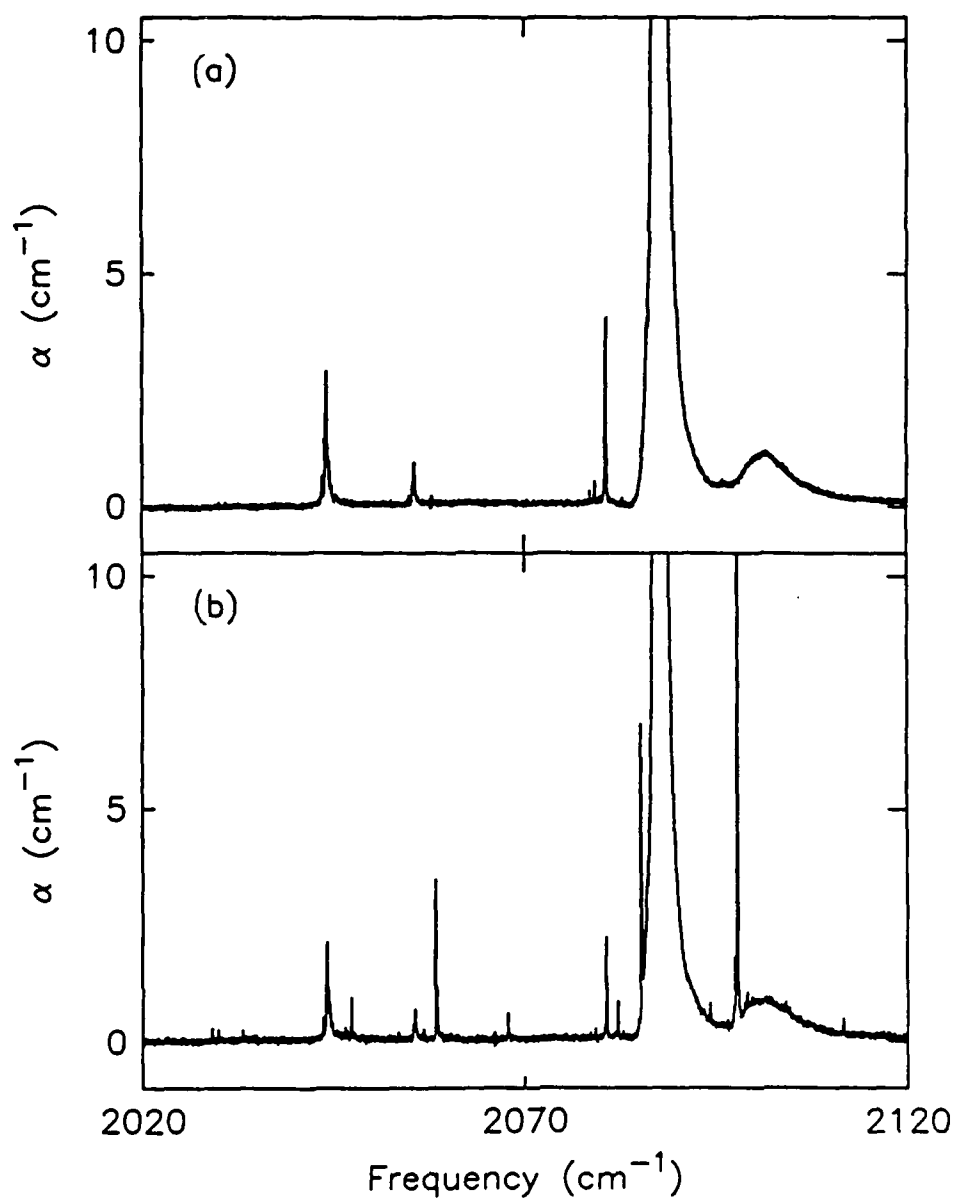
b —————

c —————



$\text{BH}_2\text{D}_2^-$





TECHNICAL REPORT DISTRIBUTION LIST, GEN

	<u>No. Copies</u>		<u>No. Copies</u>
Office of Naval Research Attn: Code 1113 800 N. Quincy Street Arlington, Virginia 22217-5000	2	Dr. David Young Code 334 NORDA NSTL, Mississippi 39529	1
Dr. Bernard Douda Naval Weapons Support Center Code 50C Crane, Indiana 47522-5050	1	Naval Weapons Center Attn: Dr. Ron Atkins Chemistry Division China Lake, California 93555	1
Naval Civil Engineering Laboratory Attn: Dr. R. W. Drisko, Code L52 Port Hueneme, California 93401	1	Scientific Advisor Commandant of the Marine Corps Code RD-1 Washington, D.C. 20380	1
Defense Technical Information Center Building 5, Cameron Station Alexandria, Virginia 22314	12 high quality	U.S. Army Research Office Attn: CRD-AA-IP P.O. Box 12211 Research Triangle Park, NC 27709	1
DTNSRDC Attn: Dr. H. Singerman Applied Chemistry Division Annapolis, Maryland 21401	1	Mr. John Boyle Materials Branch Naval Ship Engineering Center Philadelphia, Pennsylvania 19112	1
Dr. William Tolles Superintendent Chemistry Division, Code 6100 Naval Research Laboratory Washington, D.C. 20375-5000	1	Naval Ocean Systems Center Attn: Dr. S. Yamamoto Marine Sciences Division San Diego, California 91232	1

END 12-86

DTIC